AIRCRAFT AND DIFFERENTIAL FLATNESS

Yirmeyahu Kaminski, François Ollivier

▶ **To cite this version:**

Yirmeyahu Kaminski, François Ollivier. AIRCRAFT AND DIFFERENTIAL FLATNESS. 2022. hal-03680676v1

HAL Id: hal-03680676

https://hal.science/hal-03680676v1

Preprint submitted on 28 May 2022 (v1), last revised 27 Mar 2024 (v6)

HAL is a multi-disciplinary open access archive for the deposit and dissemination of scientific research documents, whether they are published or not. The documents may come from teaching and research institutions in France or abroad, or from public or private research centers.

L'archive ouverte pluridisciplinaire **HAL**, est destinée au dépôt et à la diffusion de documents scientifiques de niveau recherche, publiés ou non, émanant des établissements d'enseignement et de recherche français ou étrangers, des laboratoires publics ou privés.

AIRCRAFT AND DIFFERENTIAL FLATNESS

A PREPRINT

Yirmeyahu J. Kaminski
Holon Institute of Technology
Holon, Israel
kaminsj@hit.ac.il

François Ollivier
LIX, CNRS–École Polytechnique
91128 Palaiseau Cedex, France
ollivier@lix.polytechnique.fr

May 28, 2022

Keywords: Differentially flat systems, flat singularities, flat outputs, aircraft aerodynamics models, gravity-free flight, engine failure, rudder jam, differential thrust, forward sleep landing

ABSTRACT

We investigate apparent and intrinsic singularities of a flat model of aircrafts, illustrated with numerical simulations using Python and Maple. We consider failure situations and maneuvers for which apparent singularities of the previously known flat outputs may appear, making necessary to use some of the new flat outputs we consider.

Basically, the aircraft flat outputs are x, y, z, the coordinates of the gravity center, completed with any function of the sideslip angle β, the angle of attack α, the bank angle μ and the thrust F. The choice of β was previously used, but does not allow gravity-free flight, for which μ is the best choice, as well as for decrabe maneuver. The choice of F is adapted for dead-stick landing conditions with $\beta \neq 0$, such as forward slip maneuver.

This approach also allows to replace usual control with new controls in case of failures, *e.g.* differential thrust can be used in case of rudder failure.

Our results are illustrated by numerical simulations, using realistic non linear aerodynamics models. In a first stage, we investigate the ability of the flatness based control to reject perturbations. Since flatness in that case requires some model simplification, in a second stage, we focus on model errors and show that a suitable feed-back allows to keep trajectories with the complete real model close to the trajectories planned with the simplified one.

Introduction

Aims of this paper

We continue the investigation of intrinsic and apparent singularities of flat control system [8, 9, 18, 19], initiated in our previous papers [15, 16], with an application to aircraft control. We recall that flat systems are systems for which the trajectory can be parametrized using a finite set of state functions, call *flat outputs*, and a finite number of their derivatives.

Our goal is to extend the applicability of flat motion planning to emergency situations or aerobatics maneuvers when new flat outputs and/or new controls must be used.

Cases investigated

We investigate flight situations near intrinsic singularities, that correspond basically to stalling, and apparent singularities, such as gravity-free flight, for which we propose alternative flat outputs, including bank angle μ, that may also be helpful to control aircraft roll and maintain wings-level attitude during landing with side wind (decrabe maneuver).

We also show that a set of flat outputs including the thrust F may be used when $\beta \neq 0$ and is suitable to control a slip-forward maneuver for dead-stick emergency landing [25, 26].

When control surfaces are lost or actuators damaged, alternative controls may be used [2, 3, 13, 21]. We have here investigated the use of differential thrust in the case of a damaged rudder, and also the case of a single engine lost.

Models and implementations

In our simulations, we used the aircraft model and sets of parameters provided by Grauer and Morelli [10] for various types of aircraft: fighter F16C, STOL utility aircraft DHC-6 Twin Otter and NASA Generic Transport Model (GTM), a subscale airliner model. Such aerodynamics models are not known to be flat, unless one neglects some terms, *viz.* the thrusts created by the control surfaces and related to the control functions and rotation angles.

We investigated first the robustness of the flat control with respect to some failures and some perturbations, for the simplified model, using simulations performed in Python. In a second stage, a Maple implementation was used to test the ability of a suitable feed-back to keep the trajectories of the full model close to the theoretical trajectories computed with the simplified flat one.

Plan of the paper

In sec. 1, we define flatness and flat singularities 1.1, providing some local flatness criterion 1.2. We show that the simplified aircraft is a flat chained model 1.3. The section 2 is devoted to the various possible choices of flat outputs and their singularities. The outputs x, y, z may be completed with the side-slip angle β 2.1, the bank angle μ 2.2 or the engines thrust F 2.3. Some other possibilities are also mentionned 2.4. Stalling conditions and their relations to flatness are investigated 2.5. Section 3 considers failures, such as one engine breakdown 3.1, rudder failure 3.2, forward slip with all engines lost3.3. Section 4 reports simulations using the simplified model, starting with a description of the feed-back design and the Python implementation 4.2. We first consider a single engine breakdown 4.3, then initial perturbations 4.4 and the effect of constant and variable wind 4.5. The last section 5 reports experiments with the full model with a Maple implementation 5.1. We start with the F-16C model near stalling conditions 5.2, then gravity free flight 5.3 using flat output μ, a Twin-Otter with one engine lost 5.4 or with a rudder failure 5.5. The last subsections describe a GTM landing with de-crab maneuver 5.6 using μ and forward slip maneuver 5.7 using flat output F. A nomenclature is given in appendix A and details on the aircraft models in appendix B.

1 Flatness

For more details on flat systems, we refer to Fliess *et al.* [8, 9] or Lévine [18, 19]. Roughly speaking, the solutions of flat systems are parametrized by m differentially independent functions, called flat outputs, and a finite number of their derivatives. This property, which characterize them, is specialy important for motion planning. We present here flat systems in the framework of diffiety theory [29, 30]. A full understanding of this theoretical setting is not mandatory to understand the applicational sections of the paper.

1.1 Definitions and properties

We will be concerned here with systems of the following shape:

$$x_i' = f_i(x, u, t), \text{ for } 1 \leq i \leq n, \tag{1}$$

where $x_1, \ldots, x_n$ are the state variables and $u_1, \ldots, u_m$ the controls.

In the sequel, we may sometimes denote ∂/∂_x by ∂_x, for short.

Definition 1. *A diffiety is a $\mathcal{C}^\infty$ manifold V of denumerable dimension equipped with a global derivation δ (that is a vector field), the* Cartan derivation *of the diffiety. The ring of function $\mathcal{O}(V)$ is the ring of $\mathcal{C}^\infty$ function on V depending on a* finite *number of coordinates. The topology on the diffiety is the coarsest topology that makes coordinate functions continuous, i.e. the topology defined by open sets on subspaces of finite dimensions.*

The trivial diffiety $\mathbf{T}^m$ *is* $\left(\mathbb{R}^{\mathbb{N}}\right)^m$ *equipped with the derivation* $\delta := \sum_{i=1}^m \sum_{k\in\mathbb{N}} z_i^{(k+1)} \partial/\partial_{z_i^{(k+1)}}$.

A morphism of diffiety $\phi : V_1 \mapsto V_2$ is a smooth map between manifolds such that $\phi^* \circ \delta_2 = \delta_1 \circ \phi^*$, where $\phi^* : \mathcal{O}(V_2) \mapsto \mathcal{O}(V_1)$ is the dual application, defined by $\phi^*(f) = f \circ \phi$ for $f \in \mathcal{O}(V_2)$.

A diffiety V is flat if there exists a dense open set $W \subset V$ of flat points*. In that context a point is called flat, if it admits a neighborhood that is diffeomorphic to an open set of $\mathbf{T}^m$. The generators z_i of $\mathbf{T}^m$ are called* linearizing outputs *or* flat outputs. [1]

A set of such flat outputs defines a Lie-Backlünd atlas, as defined in [15].

A point in called singular if no flat output is defined in a neighborhhod of it. If an existing flat ouput can be extended to this point, it is called an apparent singularity. Otherwise it is called an intrinsic singularity.

We illustrate this definition by associating a diffiety to the system considered above.

Example 2. *Any system* (1) *diffines a diffiety $U \times \left(\mathbb{R}^{\mathbb{N}}\right)^m$, where $U \subset \mathbb{R}^{n+m+1}$ is the domain of definition of the functions f_i, equipped with the Cartan derivation*

$$\frac{\mathrm{d}}{\mathrm{d}t} := \partial_t + \sum_{i=1}^{n} f_i(x,u,t)\partial_{x_i} + \partial_{j=1}^{m} \sum_{k\in\mathbb{N}} u_j^{(k+1)} \partial_{u_j^{(k)}} \tag{2}$$

Flatness may be illustrated by the classical car example.

Example 3. *A very simplified car model is the following:*

$$\left\{ \begin{array}{rcl} \dot{x} & = & u\cos\theta \\ \dot{y} & = & u\sin\theta \\ \dot{\theta} & = & \frac{u}{\ell}\tan\varphi \end{array} \right. \tag{3}$$

The state vector is made of the coordinates (x, y) of the rear axle's center and of the angle θ between the car's axis and the x-axis. The controls are the speed u and the angle φ between the wheels' axis and the car's axis. The length ℓ is the distance between the two axles.

One can define different sets of flat outputs depending on the actual open set, where they are defined, as follows.

1. *Over $U_1 = \{\dot{x} \neq 0\}$, we take $z_{(1)} = (x, y) = \psi_1(\mathfrak{x})$ and the inverse Lie-Bäcklund transform is given by:*

$$\phi_1 = \begin{pmatrix} x \\ y \\ \tan^{-1}(\frac{\dot{y}}{\dot{x}}) \end{pmatrix}$$

2. *Over $U_2 = \{\dot{y} \neq 0\}$, we take $z_{(2)} = (x, y) = \psi_2(\mathfrak{x})$ and the inverse Lie-Bäcklund transform is given by:*

$$\phi_2 = \begin{pmatrix} x \\ y \\ \mathrm{cotan}^{-1}(\frac{\dot{x}}{\dot{y}}) \end{pmatrix}$$

3. *Over $U_3 = \{\dot{\theta} \neq 0\}$, we take $z_{(3)} = (\theta, x\sin\theta - y\cos\theta) = \psi_3(\mathfrak{x})$. Here for the sake of simplicity, we shall denote (z_1, z_2) the components of $z_{(3)}$. In that case, the inverse Lie-Bäcklund transform is given by:*

$$\phi_3 = \begin{pmatrix} \frac{\dot{z}_2}{\dot{z}_1}\cos z_1 + z_2 \sin z_1 \\ \frac{\dot{z}_2}{\dot{z}_1}\sin z_1 - z_2 \cos z_1 \\ z_1 \end{pmatrix}$$

See [15] for all the details.

1.2 Local flatness condition.

The linearized tangent system of (1) at a point (x_0, u_0) is classically defined as:

$$\dot{\delta x} = \frac{\partial f}{\partial x}(x_0, u_0)\delta x + \frac{\partial f}{\partial u}(x_0, u_0)\delta u.$$

[1] Making this high flown terminology more concrete, this means that both the state and input variables x_i, u_i are functions of the z_i and a finite number of their derivatives on one hand. On the other hand, this also means that the z_i are functions of the state and input variables and a finite number of their derivatives, and that the differential dz_i are linearly independent.

When working in the framework of diffieties, one has to add to this system all other systems that are deduced from it appliying the Cartan derivation of the diffiety. This leads to the formal point of view introduced here, just for the sake of completeness.

Definition 4. *Let η be a point of a diffiety V. For any function $g \in \mathcal{O}(V)$, we denote by $\mathrm{j}_\eta(g)$ the power series $\sum_{k\in\mathbb{N}} g^{(k)}(\eta)\tau^k$.*

For any system Σ defined by (1)*, we define the* linearized system at the point η*, denoted by $\mathrm{d}_\eta\Sigma$, to be*

$$\mathrm{d}\dot{x}_i = \sum_{i=1}^{n} \mathrm{j}\frac{\partial f_i(x,u)}{\partial x_i}\mathrm{d}x_i + \sum_{j=1}^{m} \mathrm{j}\frac{\partial f_i(x,u)}{\partial u_j}\mathrm{d}u_j. \tag{4}$$

There exists a whole algebraic approach to flat systems and their linear tangent systems. For details, we refer to [7]. We will limit ouselves here to mention that for a flat system, the module generated by the differentials of the flat outputs is free, as stated by the following lemma, which provides a necessary condition for local flatness.

Theorem 5. *At any flat regular point η, the linearized system defines a free module.*

PROOF. — For a linear system, controlable means flat: from the algebraic standpoint, the associated *module* is *free*, which just means that it is generated by a *basis*. If z is a flat output, then at any flat point η, $\mathrm{d}_\eta z$ is a basis of the module defined by the linearized system. Indeed, for any function $H(z)$ depending on z and its derivatives up to order r, we have

$$\mathrm{d}H(z) = \sum_{i=1}^{m}\sum_{k=0}^{r} \frac{\partial H}{\partial z_i^{(k)}}\mathrm{d}z_i^{(k)},$$

so that it is a linear combination of derivatives of the $\mathrm{d}z_i$. ∎

1.3 The simplified aircraft. A chained model

We study here the model without going into the details of the equation, which are completely described in annex B.

1.3.1 Description of the model

Controls In the given model, the dynamic of actuators is neglected and the controls actually depend on five physical quantities: the thrust of the engines F_1 and F_2, and virtual angles δ_l, that corresponds to ailerons, δ_m, that corresponds to elevators and δ_n, that corresponds to the rudder. In a regular flight, $F_1 = F_2$, and we shall use the total thrust $F = F_1 + F_2$ whose torque with respect to G is close to zero and is negligible. Then we have four physical inputs: $F, \delta_l, \delta_m, \delta_n$.

Assuming a rudder failure, the command δ_n may be lost. Then, we may use differential thrust and replace this command with $\eta := (F_1 - F_2)/(F_1 + F_2)$. In order to model a single engine breakdown, one may set $\eta = \mp 1$. See subsections 4.3 and 5.4. When considering a single engine aircraft, such as the F-16, one sets $\eta = 0$, which is the default value in implementations. See subsection 5.3.

The 12 state variables are (x, y, z), the coordinates of the center of gravity, γ, the flight path angle, χ, the heading angle, V, the aircraft speed, α, the angle of attack, β, the sideslip angle, μ, the bank angle and (p, q, r) the angular speed vector. Enlarging the state with F, $\dot{F}$ and $\ddot{F}$, we may divide the state variables in 4 sets, completed with a 5^{th} set:

$$\begin{array}{rcl}
\Xi_1 & := & (\xi_{1,1} := x, \xi_{1,2} := y, \xi_{1,3} := z), \\
\Xi_2 & := & (\xi_{2,1} := V, \xi_{2,2} := \chi, \xi_{2,3} := \gamma), \\
\Xi_3 & := & (\xi_{3,1} := \alpha, \xi_{3,2} := \beta, \xi_{3,3} := \mu, \xi_{3,4} := F), \\
\Xi_4 & := & (\xi_{4,1} := p, \xi_{4,2} := q, \xi_{4,3} := r, \xi_{4,4} := \dot{F}), \\
\Xi_5 & := & (\xi_{5,1} := \delta_l, \xi_{5,2} := \delta_m, \xi_{5,3} := \delta_n, \xi_{5,4} := \ddot{F}).
\end{array} \tag{5}$$

The aircraft equations (24a–24i,25) depend on the forces (X, Y, Z) (23a–23c) and torques (L, M, N) (23d–23f), that respectively depend on the aerodynamic forces F_a (22a) and aerodynamic torques T_a (22b). These functions depend on the aircraft geometry. In our simulations, we used the values provided by the GNA model. See B.3.

The expression of F_a actually depends on the δ_i and also on p, q and r, but this dependency can be, to some extend, neglected. We then get the simplified aircraft system, which is of the form

$$\Xi_i' = f(\Xi_1, \ldots, X_{i+1}), \text{ for } 1 \le i \le 4. \tag{6}$$

The general shape of equations remains the same if δ_n is replaced by η, to use differential thrust in case of rudder failure. So, we have a chained model. In the generic case, the state functions and controls can be computed knowing (x, y, z) and their derivatives up to order 4 and some function $\zeta(\alpha, \beta, \mu, F)$ and its derivatives up to order 2. We show in appendix B.4 that this actually stands on some dense open subset of the state space. Actually, we need to assume $\cos(\gamma) \neq 0$, due to the choice of Euler angles γ and χ. Other choices would be possible, necessitating a change of charts for aerobatics, an issue not considered here.

In fact, the expression of the derivatives of Ξ_i, depending on Ξ_{i+1} is linear for $\in \{1, 3, 4\}$. See app. B.4. The main point is then to be able to compute Ξ_3, knowing Ξ_2', and some extra flat output $\zeta(\alpha, \beta, \mu, F)$. The flat points for the choice of flat output $\zeta = \beta$, $\zeta = \mu$ and $\zeta = F$ are discussed in section 2.

This means that instead of solving the differential equations (24a–24i,25), we can compute solutions, parametrized by choosing arbitrary time varying functions for the flat outputs: $x = \hat{x}(t)$, $y = \hat{y}(t)$, $z = \hat{z}(t)$ and $\mu = \hat{\mu}(t)$, in the dense open space where some inequalities are satisfied. Such a property characterizes *flat systems*, according to the formalism in subsec. 1.1.

Example 6. *We can associate a diffiety to our aircraft model, which is defined by* $\mathbb{R}^{12} \times \left(\mathbb{R}^{\mathbb{N}}\right)^4$*, and a derivation* $\eth$ *defined by* $\eth := \eth_0 + \eth_1$*, where* $\eth_1$ *is the trivial derivation on* $\left(\mathbb{R}^{\mathbb{N}}\right)^4$*:* $\eth_1 := \sum_{z\in\{F,\delta_l,\delta_m,\delta_n\}}^{m} \sum_{k\in\mathbb{N}} z_i^{(k+1)} \partial/\partial z_i^{(k+1)}$ *and* $\eth_0$ *is defined on* $\mathbb{R}^{12}$ *by the differential equations (24a–24i,25):*

$$\delta_0 := V(t)\cos(\chi(t))\cos(\gamma(t))\frac{\partial}{\partial x} + V(t)\sin(\chi(t))\cos(\gamma(t))\frac{\partial}{\partial y} + \cdots$$

It is flat, as in the dense open set where inequation (9) *below stands, we may choose* x*,* y*,* z*,* μ *and their derivatives as new coordinates, which makes the diffiety isomorphic to an open subset of* $\mathbf{T}^4$*.*

In practice, the diffiety is a smaller open set. The values of the controls are bounded and one wishes to restrict the values of attack angle α *or side-slip angle* β *for safety reasons. The maximal values for the GNA model are given below* (26)*. Other limitations must be included, such as the maximal value of the thrust. The speed* V *should also be greater than the stallin speed (see 2.5).*

We will not insist any more on the theoretical setting of diffiety theory.

2 Choices of flat outputs

Easy considerations in app. B.4 reduce the problem of the flat motion planning computation to the expression of α, β, μ and F as local functions of X, $\sin\mu\, Y + \cos\mu\, Z$, $\cos\mu\, Y - \sin\mu\, Z$ and ζ, provided that $\dot{x}^2 + \dot{y}^2 \neq 0$, an hypothesis satified in regular flight conditions.

2.1 The side-slip angle choice

Martin [23, 24] has used the set of flat outputs: x, y, z, β. We need to explicit under which condition such a flat output may be chosen, *i.e.* when the Jacobian determinant

$$D_1 := \begin{vmatrix} \frac{\partial X}{\partial \alpha} & \frac{\partial X}{\partial \mu} & \frac{\partial X}{\partial F} \\ \frac{\partial(\sin\mu\, Y + \cos\mu\, Z)}{\partial \alpha} & \frac{\partial(\sin\mu\, Y + \cos\mu\, Z)}{\partial \mu} & \frac{\partial(\sin\mu\, Y + \cos\mu\, Z)}{\partial F} \\ \frac{\partial(\cos\mu\, Y - \sin\mu\, Z)}{\partial \alpha} & \frac{\partial(\cos\mu\, Y - \sin\mu\, Z)}{\partial \mu} & \frac{\partial(\cos\mu\, Y - \sin\mu\, Z)}{\partial F} \end{vmatrix}$$

does not vanish. First, we remark, following Martin [23, p. 80] that when $Y = gm\cos(\gamma)\sin(\mu)$ and $Z = gm\sin(\gamma)\sin(\mu)$, *i.e.* when the lift is zero, $\sin\mu\, Y + \cos\mu\, Z = gm\cos(\gamma)$ and $\cos\mu\, Y - \sin\mu\, Z = 0$, so that the last row of D_1 is zero and the determinant vanish. This mean that 0-g flight trajectories are singular for this flat output. On the other hand, when β and α are close to 0, which is the case in straight and level flight, easy computations using eq. (23a–23c) allow Martin to conclude that

$$D_1 \approx -Z\left(\frac{\rho}{2}SV^2\frac{\partial C_z}{\partial \alpha} + F\right) \gg 0.$$

To go further, one may use the expression of X eq (23a) and deduce from it

$$F = \frac{X + \frac{\rho}{2}SV^2C_x + gm\sin(\gamma)}{\cos(\alpha+\epsilon)\cos(\beta)}, \tag{7}$$

assuming $\cos(\alpha+\epsilon)\cos(\beta)$. Substituting this expression in Y and Z, we define $\tilde{Y}$ and $\tilde{Z}$ and further define $\hat{Y} := \cos(\mu)\tilde{Y} - \sin(\mu)\tilde{Z}$ and $\hat{Z} := \sin(\mu)\tilde{Y} + \cos(\mu)\tilde{Z}$. Then, $D_1 \neq 0$ when

$$\begin{vmatrix} \frac{\partial \hat{Y}}{\partial \alpha} & \frac{\partial \hat{Y}}{\partial \mu} \\ \frac{\partial \hat{Z}}{\partial \alpha} & \frac{\partial \hat{Z}}{\partial \mu} \end{vmatrix} \neq 0. \tag{8}$$

The main interest of this choice is to be able to impose easily $\beta = 0$, which is almost always required.

2.2 The bank angle choice

As the angle μ is known, we may compute from Ξ_1' and Ξ_1'' the values X, Y and Z. So, singularities for this flat outputs are such that

$$D_2 := \begin{vmatrix} \frac{\partial X}{\partial \alpha} & \frac{\partial X}{\partial \beta} & \frac{\partial X}{\partial F} \\ \frac{\partial Y}{\partial \alpha} & \frac{\partial Y}{\partial \beta} & \frac{\partial Y}{\partial F} \\ \frac{\partial Z}{\partial \alpha} & \frac{\partial Z}{\partial \beta} & \frac{\partial Z}{\partial F} \end{vmatrix} \neq 0 \tag{9}$$

Using $\tilde{Y}$ and $\tilde{Z}$, as defined in subsec. 2.1, we see that this is equivalent to

$$\begin{vmatrix} \frac{\partial \hat{Y}}{\partial \alpha} & \frac{\partial \hat{Y}}{\partial \beta} \\ \frac{\partial \hat{Z}}{\partial \alpha} & \frac{\partial \hat{Z}}{\partial \beta} \end{vmatrix} \neq 0. \tag{10}$$

When β is 0, $\partial\tilde{Z}/\partial\beta$ is also 0, due to the aircraft symmetry. Using the GNA model (see B.3), we have $\partial C_x/\beta = 0$ and $\partial C_z/\partial\beta = 0$, so that $\partial\tilde{Z}/\partial\beta = 0$. The value of the determinant (10) is then

$$-\frac{\partial \hat{Z}}{\partial \alpha}\frac{\partial \hat{Y}}{\partial \beta}. \tag{11}$$

For most aircrafts, $\partial C_y/\partial\beta$ is negative at $\beta = 0$, with values in the range $[-1., -0.5]$. Delta wing aircrafts seem to be a exception, with smaller absolute values (-0.014 for the X-31) or even negative ones ($+0.099$ for the F-16XL). It seems granted that for regular transport planes, $\partial C_y/\partial\beta$ is negative, so that the determinant vanishes only when $\partial\tilde{Z}/\partial\alpha$ is 0. We will see in 2.5 that this may be interpreted as stalling condition and that the vanishing of (11) on a trajectory with constant controls means that the points of this trajectory are flat singularities, so that no other flat outputs could work.

This choice is the best to impose $\mu = 0$ and is natural for decrabe maneuver, that is when landing with a lateral wind, which implies $\beta \neq 0$. We then need to maintain μ close to 0 to avoid the wings hiting the runway. See subsection 5.6 below.

It is also a good choice when $Y = Z = 0$, a situation that may be encountered in aerobatics or when training for space condition with 0-g flights (see subsec 5.3). The two choices are compared in subsec. 5.4 with the simulation of a twin otter flying with one engine.

2.3 The thrust choice

The choice of thrust F has one main interest: to set $F = 0$ and consider the case of a aircraft having lost all its engines. The singularities of this flat output are such that

$$D_3 := \begin{vmatrix} \frac{\partial X}{\partial \alpha} & \frac{\partial X}{\partial \mu} & \frac{\partial X}{\partial \beta} \\ \frac{\partial(\sin\mu\, Y + \cos\mu\, Z)}{\partial \alpha} & \frac{\partial(\sin\mu\, Y + \cos\mu\, Z)}{\partial \mu} & \frac{\partial(\sin\mu\, Y + \cos\mu\, Z)}{\partial \beta} \\ \frac{\partial(\cos\mu\, Y - \sin\mu\, Z)}{\partial \alpha} & \frac{\partial(\cos\mu\, Y - \sin\mu\, Z)}{\partial \mu} & \frac{\partial(\cos\mu\, Y - \sin\mu\, Z)}{\partial \beta} \end{vmatrix}$$

vanishes. When $F = 0$, by eq. (23a–23c), the vanishing of D_3 is equivalent to

$$\begin{vmatrix} \frac{\partial C_x}{\partial \alpha} & 0 & \frac{\partial C_x}{\partial \beta} \\ \frac{\partial(\cos\mu\, C_z)}{\partial \alpha} & \frac{\partial(\sin\mu\, C_y + \cos\mu\, C_z)}{\partial \mu} & \frac{\partial(\sin\mu\, C_y)}{\partial \beta} \\ \frac{\partial(-\sin\mu\, C_z)}{\partial \alpha} & \frac{\partial(\cos\mu\, C_y - \sin\mu\, C_z)}{\partial \mu} & \frac{\partial(\cos\mu\, C_y)}{\partial \beta} \end{vmatrix} = \frac{\partial C_x}{\partial \alpha}\left(C_y\frac{\partial C_y}{\partial \beta} - C_z\frac{\partial C_x}{\partial \beta}\right).$$

When β vanishes, C_y and $\partial C_z/\partial\beta$ also vanish, due to the aircraft symmetry with respect to the xz-plane. So, we need have $\beta \neq 0$ to use those flat outputs. Using the GNA model, C_x and C_z depend only on α and C_y depends linearly on β.

In the case of a gliding aircraft, situations with $\beta \neq 0$ could precisely be usefull to achieve the forward slip maneuver. See subsection 3.3.

2.4 Other sets of flat outputs

Among the other possible choices for completing the set Ξ_1 in order to get flat outputs, α does not seem to have much specific interest. One may also consider time varying expressions, e.g. linear combinations of β and μ, to smoothly go from one choice to another.

2.5 Stalling conditions

It is known that the lift of a wing reaches a maximum at a critical angle of attack, due to flow separation. This phenomenon can be hardly reversible and create a sudden drop of the lift force Z from its pick value. Our mathematical model is too poor to fully reflect such behaviour, but a maximum for the lift can still be computed.

We need to take also in account the contribution of the thrust in the expression of Z, and simple computations show that the critical angle of attack corresponds in our setting to a maximum of $\tilde{Z}$, that is $\partial\tilde{Z}/\partial\alpha = 0$, which corresponds to the singularity for flat output μ already observed above (11).

Three cases may appear with stalling:

1) to reach an extremal value of $\tilde{Z}$, meaning that $\partial\tilde{Z}/\partial\alpha$ vanishes;

2) to reach the maximum thrust $F_{\max}$ before reaching a maximum of $\tilde{Z}$;

3) reaching no maximum of $\tilde{Z}$ with a aircraft with trust/weight ratio greater than 1: in such a case, there is no stalling.

For horizontal straight line trajectories, we may compute the speed V and the thrust F, depending on α, for $\beta = \mu = 0$, using the simplified model. We may also use the full model. As α, β and μ are constants, $p = q = r = 0$, which further allows to express δ_ℓ, δ_m and δ_n depending on α, so that $C_\ell = C_m = C_n = 0$, which is easy with the GNA model that is linear in those quantities.

E.g., For the F4, setting the weight to 38924lb [10], the evaluated stall speed, angle of attack and thrusts are respectively 67.6789m/s (131.56kn), 0.4200rad (24.07°) and 77.0436 for the full model and 64.0904m/s, 0.4366rad and 78.8806 for the simplified one, without thrust limitations. These thrust values are bellow the thrust of J79-GE-17A engines of later versions (79.38kN with afterburning). Assuming a maximal thrust of 2×71.8kN, that corresponds to the J79-GE-2 engines of the first production aircrafts, the stall speed and angle of attack are 67.9835m/s and 0.3969rad with the full model, 64.5515m/s and 0.4057rad with the simplified one. The full model stall speed of about 132kn agrees more or so with the stall speed values of 146KCAS or 148KCAS, according to the models, computed with the NATOPS manual [27, fig. 4.1 and 4.2] at 10000 ft and below and the computed a.o.a of 23° with the indicated stall a.o.a of 27 to 28 "units", keeping in mind that those units are not exactly degrees and that our mathematical definition of stalling cannot fully match the actual behaviour. See fig. 1.

Figure 1: F-4: values of V and F depending on α, for the real (left) and simplified models (right)

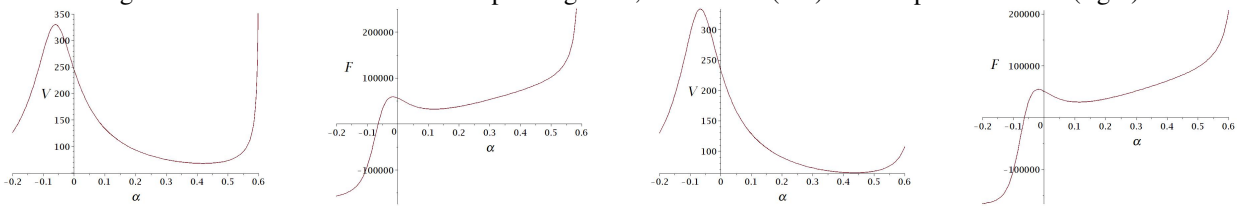

The case of the F-16C is considered in 5.2.

We now address the relation of stalling with controlability.

Theorem 7. *Consider a trajectory such that γ and μ are constants. If $\partial\tilde{Z}/\partial\alpha$ is equal to 0, then this trajectory is not flat.*

PROOF. — The equality $\partial\tilde{Z}/\partial\alpha = 0$ implies that, using the linearized equations corresponding to equations (24e&24f), as in th. 5, we have $(\cos\mu \mathrm{d}\gamma - \sin\mu\cos\gamma \mathrm{d}\chi)' = 0$. So, $(\cos\mu \mathrm{d}\gamma - \sin\mu\cos\gamma \mathrm{d}\chi$ is a non trivial torsion element, so the module is not free and the system is not flat, according to th. 5. ∎

This shows that the condition of regularity for the flat output μ, that imply to $\partial\tilde{Z}/\partial\alpha \neq 0$ under reasonnable hypotheses (see (11)) is in fact a necessary flatness condition.

3 Failures

We shall consider three types of failures:

1. single engine breakdown,
2. rudder failure,
3. all engines breakdown.

3.1 A single engine breakdown

In case of a single reactor failure, the force F will be limited to one of the F_i's. The total force variables X, Y, Z are not affected, whereas the torques L, M, N are. Without loss of generality, we shall assume that the remaining propulsion force is F_1. This situation suits the formalism of subsection 1.3. With the simplified model, for a straight trajectory, choosing $\beta = 0$ or $\mu = 0$ makes no difference, but they cannot be both 0 with the full model, mostly due to the additional lateral thrust induced by the rudder action δ_n necessary to balance the torque created by the single thrust F_1. This is investigated in subsection 5.4.

3.2 Rudder failure

Rudder failure is a classical situation where differential thrust is known to have been applied with success, which requires that the engines are not used at maximal power during take-off and/or themselves lost. Classical examples include Americal Airlines Flight 96 [25] or 2003 Baghdad DHL attempted shootdown incident [5]. One must notice that in those two cases, the elevators control was lost too, making the attitude control more difficult, an issue that is not addressed here. See also on this topic [2, 3, 13, 21].

3.3 Forward slip with all engines lost

The aircraft must land by gliding when all engines are lost. This is a rare situation, but many successfull examples are known, including the famous US Airways Flight 1549 [26]. We have seen that our flat output requires $\beta \neq 0$, whereas β should be close to 0 if one wishes to avoid a too fast descent.

But when the aircraft is too high, combining non zero β and μ precisely allows a fast descent while keeping a moderate speed. This is very usefull when gliding, as there is no option for a go around when approaching the landing strip too high or too fast. This maneuver was performed with success by the "Gimli Glider" [20], Air Canada Flight 143, that ran out of fuel on July 23, 1983, which could land safely in Gimli former Air Force base [20]. A simulation of the forward slip is provided in subsection 5.7.

4 Simulations using the simplified flat model

In this section, we show simulations done with the flat approximation of the model. These simulations are conducted with the classical set of flat outputs described in section 2.1, that is x, y, z, β.

As mentioned above, the flat approximation consists in neglecting the dependency of C_x, C_y, C_z on $p, q, r, \delta_l, \delta_m, \delta_n$. While this approximation, at first sight, may result in some noticeable divergence from the real aircraft, we show here that the model remains robust to various perturbations in the expression of the forces.

This tends to show that in many contexts the flat approximation is quite sufficient.

Moreover, we show that the flat model allows a high flexibility in trajectory planning and tracking.

All these suitable properties remain when one reactor is out of order.

4.1 Theoretical setting for feed-back design

The great advantage of flatness is that the flat motion planning makes an open loop control immediately available. When a closed loop is required, the feedback is designed from the difference between the actual values of the flat outputs and their reference values, so that this difference, being the solution of some differential equation, tends to zero.

In the framework of the flat aircraft model, the feedback is done is two stages. Indeed the dependency of the system variables on F, p, q, r has a slow dynamics in comparison to the rapidity of the dynamics that controls p, q, r from $\delta_l, \delta_m, \delta_n$. This allows to construct a cascade feedback, as done in [24]. More precisely, one can build a dynamic

linearizing feedback that allows controlling the partial state vector $\Xi = (x, y, z, V, \alpha, \beta, \gamma, \chi, \mu, F)$ using the command $\dot{F}, p, q, r$, which allows following the reference trajectories of the flat outputs x, y, z, β, using static linearizing feedback. More precisely, one can compute a vector valued function Δ_0 and a matrix valued function Δ_1, both depending on $x, y, z, V, \alpha, \beta, \gamma, \chi, \mu, F$ such that:

$$\begin{pmatrix} x^{(3)} \\ y^{(3)} \\ z^{(3)} \\ \dot{\beta} \end{pmatrix} = \Delta_0 + \Delta_1 \begin{pmatrix} p \\ q \\ r \\ \dot{F} \end{pmatrix}$$

At this stage, the variables $p, q, r, \dot{F}$ are seen as commands. In order to make the system linear, one introduces a new vector valued command v, such that:

$$\begin{pmatrix} p \\ q \\ r \\ \dot{F} \end{pmatrix} = \Delta_1^{-1}(v - \Delta_0)$$

Eventually the command v is chosen of the form:

$$v(t) = \begin{pmatrix} P_0(x_{ref}(t) - x(t)) + P_1(\dot{x}_{ref}(t) - \dot{x}(t)) + P_2(\ddot{x}_{ref}(t) - \ddot{x}(t)) + P_3 x^{(3)}_{ref}(t) \\ P_0(y_{ref}(t) - y(t)) + P_1(\dot{y}_{ref}(t) - \dot{y}(t)) + P_2(\ddot{y}_{ref}(t) - \ddot{y}(t)) + P_3 y^{(3)}_{ref}(t) \\ P_0(z_{ref}(t) - z(t)) + P_1(\dot{z}_{ref}(t) - \dot{z}(t)) + P_2(\ddot{z}_{ref}(t) - \ddot{z}(t)) + P_3 z^{(3)}_{ref}(t) \\ -k_1(\beta_{ref}(t) - \beta(t)) + \dot{\beta}_{ref}(t), \end{pmatrix}$$

where $P(X) = P_0 + P_1 X + P_2 X^2 + P_X^3$ is actually the following polynomial $P(X) = (X - k_1)^3$. Therefore the error function $e_s(t) = s_{ref}(t) - s(t)$ satisfies the following differential equations $P(e_s(t)) = 0$. In our experiments, $k_1 = -5$, so that $e_s(t) \underset{t \to +\infty}{\longrightarrow} 0$, for each value of s in x, y, z, β.

In a second stage the variables p, q, r are controlled through a static linearizing feedback based on $\delta_l, \delta_m, \delta_n$. This part of the system, as mentioned above, is fast in comparison to the first part. More precisely, one can compute the vector valued function Λ_0 and a matrix valued function Λ_1, both depending on $V, \alpha, \beta, p, q, r$ such that:

$$\begin{pmatrix} \dot{p} \\ \dot{q} \\ \dot{r} \end{pmatrix} = \Lambda_0 + \Lambda_1 \begin{pmatrix} \delta_l \\ \delta_m \\ \delta_n \end{pmatrix}$$

Then as previously, one introduced a new command w such that

$$\begin{pmatrix} \delta_l \\ \delta_m \\ \delta_n \end{pmatrix} = \Lambda_1^{-1}(w - \Lambda_0)$$

and

$$w = \begin{pmatrix} -k_2(p_{ref}(t) - p(t)) + \dot{p}_{ref}(t) \\ -k_2(q_{ref}(t) - q(t)) + \dot{q}_{ref}(t) \\ -k_2(r_{ref}(t) - r(t)) + \dot{r}_{ref}(t) \end{pmatrix},$$

where $k_2 = -15$ in our experiments. Therefore $s(t) - s_{ref}(t) \underset{t \to +\infty}{\longrightarrow} 0$, for $s \in \{p, q, r\}$.

The rational behind this cascade feedback is the following. The variables $(x, y, z, V, \alpha, \beta, \gamma, \chi, \mu, F)$ are slowly controlled through $\dot{F}, p, q, r$. Once the required values of p, q, r are known, they are quickly reached through the control performed with $\delta_l, \delta_m, \delta_n$. The respective values of k_1 and k_2 reflect the disparity of speed between the two dynamics.

4.2 Conventions used in our simulations

We now show a series of experiments that illustrate the strength of the flat approximation to control the aircraft in various situations. Those experiments were all performed with GTM extracted from [12]. For the sake of simplicity, we have left the model is imperial units. The implementation is made in Python, relying on the symbolic library `sympy`, the numerical array library `numpy` and the numerical integration of ODE systems from the library `scipy`.

The experiments are all about following a reference trajectory defined by the following expressions:

$$\begin{cases} x_{ref}(t) &= V_1 \cos(\pi(t - Tinitial)/(Tfinal - Tinitial)) \\ y_{ref}(t) &= V_1 \sin(\pi(t - Tinitial)/(Tfinal - Tinitial)) \\ z_{ref}(t) &= -V_2 t - 1000 \\ \beta_{ref}(t) &= 0 \end{cases},$$

where $Tinitial = 0, Tfinal = 30, V_1 = 30, V_2 = 5$. This reference trajectory is an upward helix.

4.3 Following the trajectory

The first experiment is performed assuming that one reactor is out of order. Therefore the force F has now a non-vanishing moment. But the feedback allows perfectly following the reference trajectories, despite this serious anomaly. The trajectories are rendered in figure 2.

Figure 2: The values of the GTM trajectory. The reference and the actual trajectories merge perfectly. Indeed the mean relative error of the spatial location of the aircraft along the trajectory is $3.9e-08$. As for the deviation of the actual value of β with respect to the its reference, it is indeed around 1μ. Considering p and q, we observe a slight difference due to the moment of the thrust and some oscillations.

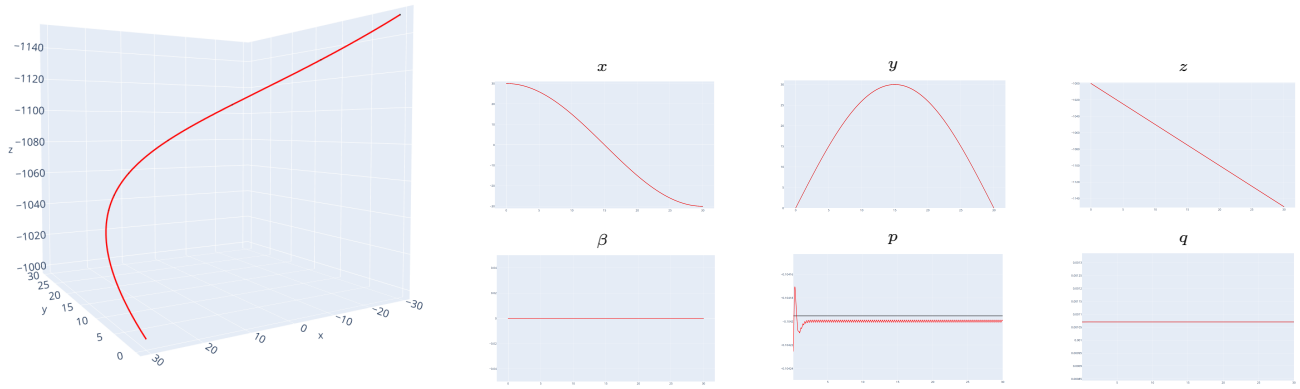

4.4 Initial perturbation

In a second stage, we carried out experiments where the aircraft started away from the reference trajectory and then joined it after a few seconds. If the initial perturbation is not too big, the feedback alone is capable to attract the aircraft to the reference trajectory. If the initial starting point is really far away from the reference trajectory, the flexibility of the flatness based approach allows designing very easily transition trajectory which can be followed with the feedback and that brings to aircraft to the reference upward helix trajectory.

In figure 3, we have rendered the actual trajectory of the aircraft and the flat outputs. It is quite apparent that when the initial perturbation is moderate, the feedback successfully brings the aircraft to the reference trajectory.

The same experiments is performed when a one reactor is broken. Again, we observe that the actual trajectory of the aircraft merges with the reference one, as shown in figure 4.

Figure 3: The values of the GTM trajectory. The reference and the actual trajectories merge perfectly, even when starting from a point off the trajectory.

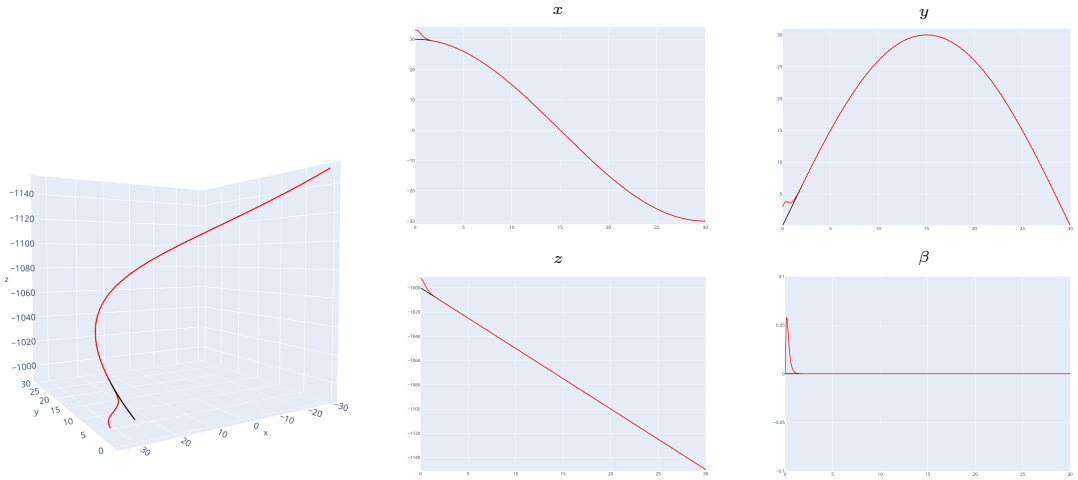

Figure 4: The values of the GTM trajectory. The reference and the actual trajectories merge perfectly, even when starting from a point off the trajectory with only one working reactor.

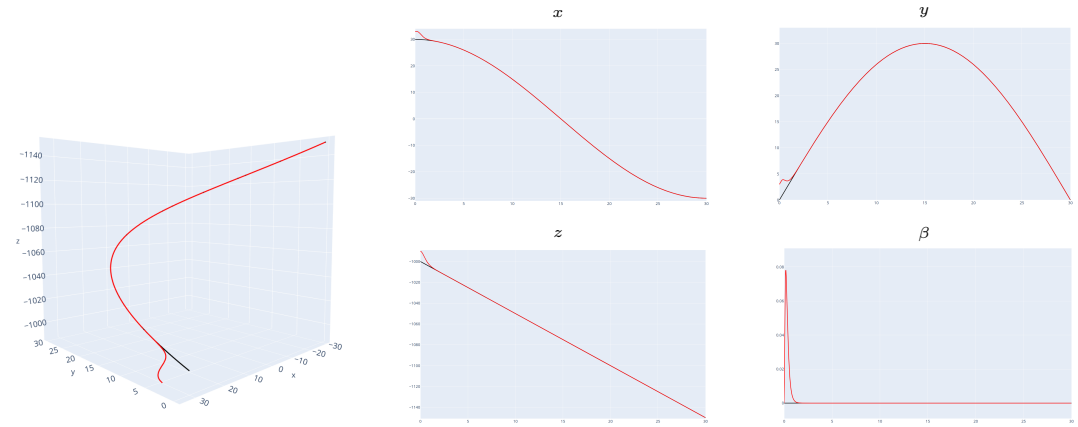

When the starting point is far away from the reference trajectory, the feedback alone cannot bring back the aircraft to it. In that case, as mentioned above, one design a transition trajectory which purpose is to connect the aircraft to the reference one. In that experiment, the aircraft start ats $p_0 = (100, -50, -1010)$ which is quite far away from the reference upward helix. We then design a polynomial transition trajectory such that it starts at p_0 and is tangent to the reference trajectory up to the order 4 at the middle of it.

This yields the following piece-wise overall reference trajectory:

$$x_{ref}(t) = \begin{cases} -9.51506609005308 \cdot 10^{-5}t^5 + 0.00713629956753981t^4 - 0.20834708393725t^3 \\ +2.95294916639042t^2 - 23.3508191089992t + 100.0 & \text{for } t < 15.0 \\ 30\cos\left(0.10471975511966t\right) & \text{otherwise} \end{cases},$$

$$y_{ref}(t) = \begin{cases} 6.66325184960611 \cdot 10^{-5}t^5 - 0.00484711621585581t^4 + 0.140903806335211t^3 \\ -2.21040529960605t^2 + 19.7718023816517t - 50.0 & \text{for } t < 15.0 \\ 30\sin\left(0.10471975511966t\right) & \text{otherwise} \end{cases}$$

and

$$z_{ref}(t) = \begin{cases} 1.31687242798354 \cdot 10^{-5}t^5 - 0.00098765432098765 4t^4 + 0.0296296296296296t^3 & \text{for } t < 15.0 \\ -0.4444444444444444t^2 - 1.66666666666667t - 1010.0 & \\ -5t - 1000 & \text{otherwise} \end{cases}$$

This piece-wise trajectory is easily tracked by the cascade feedback, as shown in figure 5. We observe a same perfect convergence between the reference and the actual trajectories, even when one reactor is broken, as it appears in figure 6.

Figure 5: The upward helix is rendered in red, while the first section of the piece-wise trajectory appears in blue. The reference and the actual trajectories merge perfectly, when the trajectory is composed of two very different pieces.

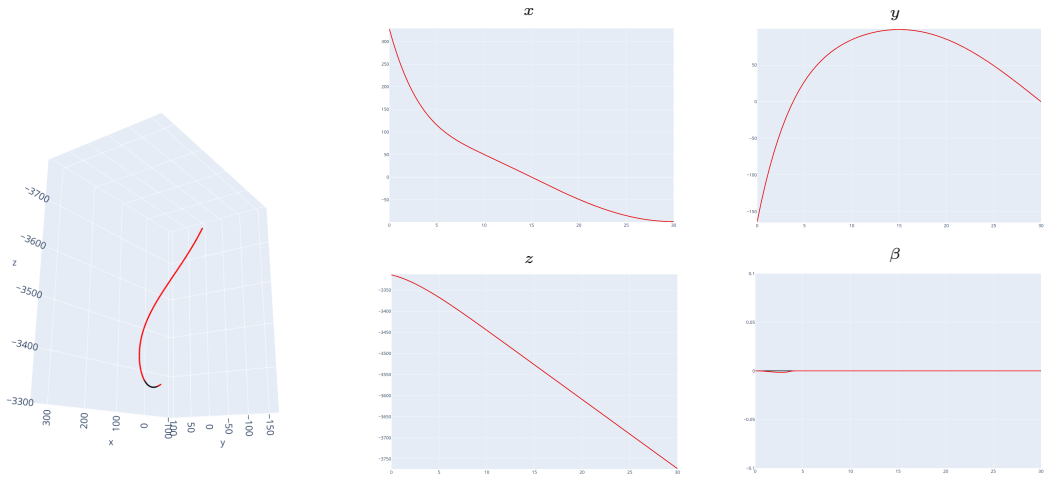

Figure 6: The upward helix is rendered in red, while the first section of the piece-wise trajectory appears in blue. The reference and the actual trajectories still merge perfectly with only one working reactor.

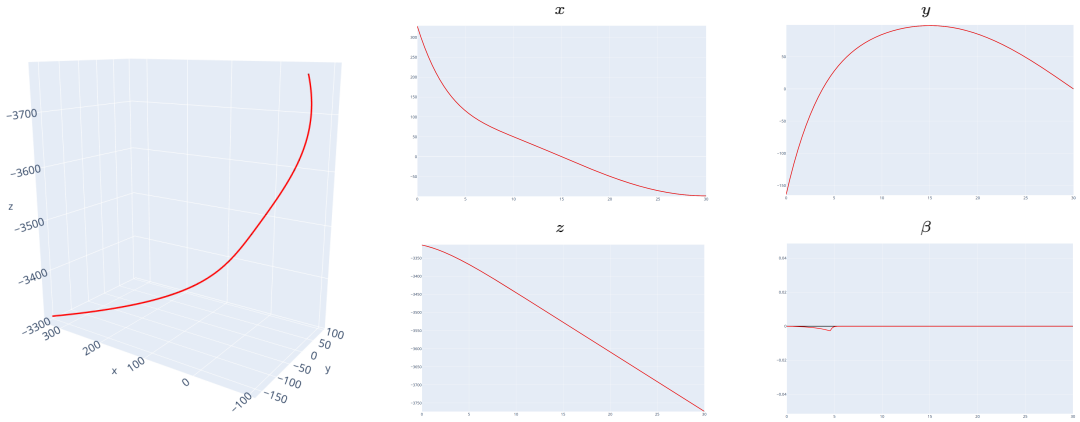

4.5 Constant and variable wind

In this section, we address the most critical problem about the flat approximation. Since the dependency of the aerodynamic coefficient on $p, q, r, \delta_l, \delta_m, \delta_n$ is discarded, one can wonder if the model is robust enough to significant perturbations in the values of the thrust. It turns out that under mild external forces, the model remains reliable.

First we consider the case of a constant wind drag of 50 lbf (222.41108 N). In this context, the feedback perfectly compensates the wind, both with two working reactors (fig. 7) and one working reactor (fig. 8).

Figure 7: Constant wind drag with two reactors. The trajectory is preserved but the wind results in a shift one can observe in the thrust, the angle μ and the angular velocities p, q, r.

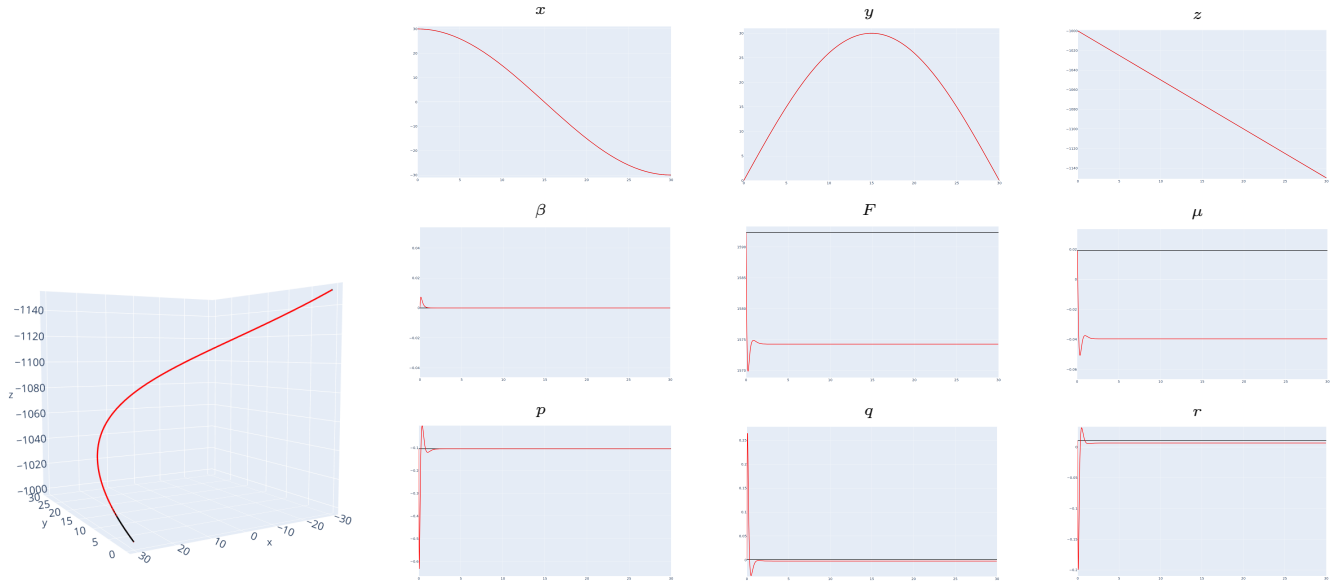

Figure 8: Constant wind drag with a single reactor. The trajectory is preserved but the wind results in a shift one can observe in the thrust, the angle μ and the angular velocities p, q, r.

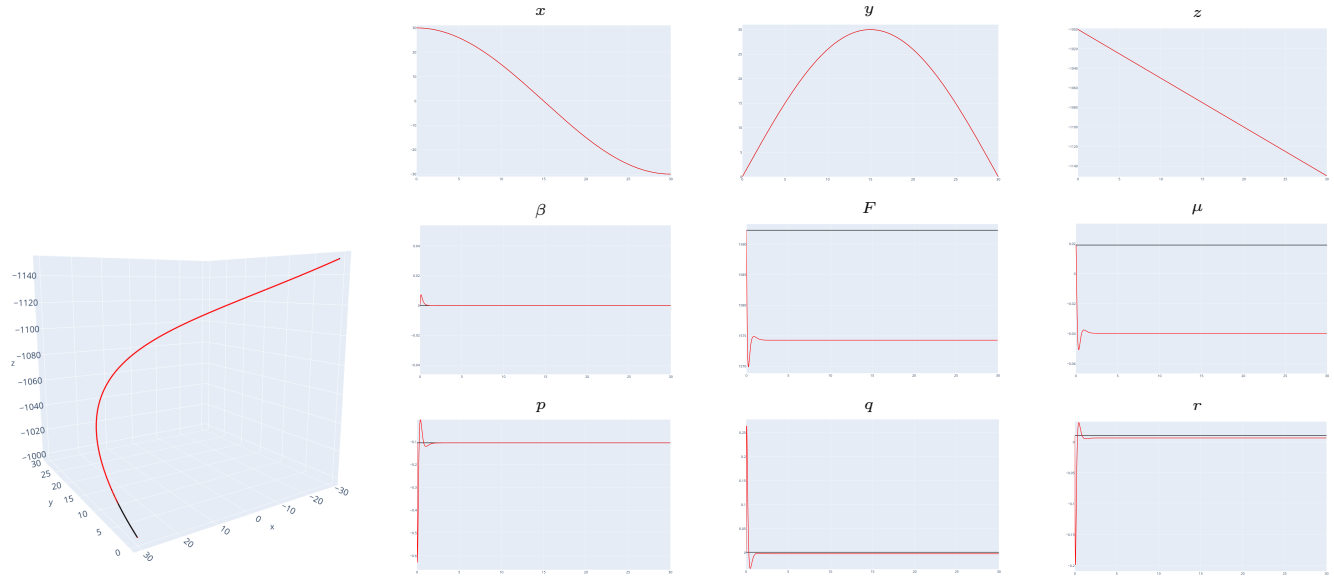

In the last experiment, the motion of the aircraft is perturbed by a variable wind. This perturbation force is a sinusoidal function which amplitude is 50lbf and frequency is 0.1Hz. This setting is applied to the GTM with the piece-wise trajectory defined above. We observe a very robust behavior of the model, as rendered in figures 9 and 10.

Figure 9: The reference and the actual trajectories still merge perfectly with a variable wind.

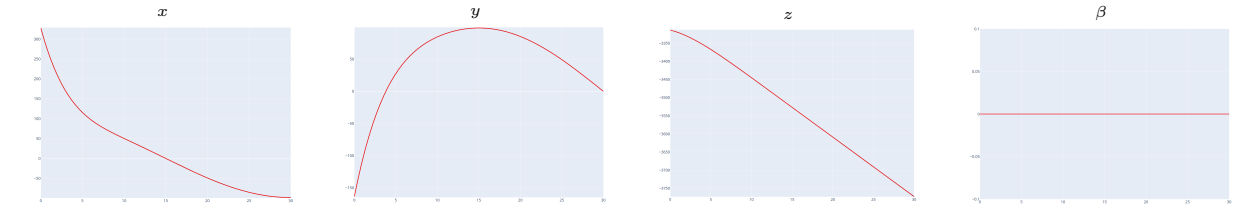

Figure 10: For the variables F, α, p, q, r variations due to the variable wind are noticeable in the graphs.

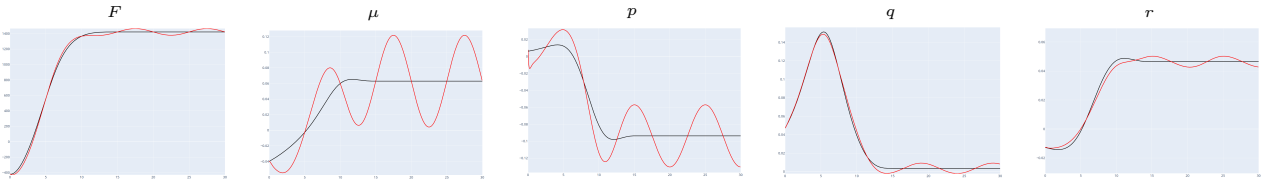

5 Simulations using the full model

5.1 Implementation in Maple

Our implementation computes power series approximations of all state variables and control at regular time interval. We proceed in the same way for the feed-back, which is also approximated with power series at the same time interval for better efficiency during numerical integration.

We denote by $\hat{\xi}(t)$ the planed function for any state variable ξ, according to the planification using the simplified flat system and the choice of $\hat{x}$, $\hat{y}$, $\hat{z}$ and $\hat{\beta}$ (or $\hat{\mu}$). We also denote by $\delta\xi$ the difference $\xi - \hat{\xi}$ between the planed trajectory and the trajectory computed with the full model. We did not manage to get a working feed-back without using integrals I_1, I_2, I_3, I_4 of $\cos(\chi)\delta x + \sin(\chi)\delta y$, $-\sin(\chi)\delta x + \cos(\chi)\delta y$, δz and $\delta\beta$ (or $\delta\mu$) respectively. When using the flat outputs x, y, z, F, I_4 is no longer needed.

For the feed-back we choose positive real numbers $\lambda_{i,j}$, with $1 \leq i \leq 4$, and $1 \leq j \leq 5$ for $i = 2$ or $i = 3$ and $1 \leq j \leq 3$ for $i = 1$ or $i = 4$. The value of δF, $\delta\delta_l$, $\delta\delta_m$, $\delta\delta_n$, are computed, so that $\prod_{i=1}^{3}(d/dt + \lambda_{1,i})I_1 = 0$, $\prod_{i=1}^{3}(d/dt + \lambda_{4,i})I_4 = 0$, $\prod_{i=1}^{5}(d/dt + \lambda_{2,i})I_2 = 0$, $\prod_{i=1}^{5}(d/dt + \lambda_{3,i})I_3 = 0$, using the derivation d/dt of the linearized simplified system around the planed trajectory. Then, we use the controls $\hat{\delta}_l + \delta\delta_l$, $\hat{\delta}_m + \delta\delta_m$, $\hat{\delta}_n + \delta\delta_n$, $\hat{F} + \delta F$ in the numerical integration. If the $\delta\xi$ are small enough to behave like the $\mathrm{d}\xi$ of the linearized system, and the solution of the full model not too far from the planed solution of the simplified model, the convergence is granted.

In practice, the choice of suitable $\lambda_{i,j}$ is difficult and empirical: two small, the trajectory is lost, two high, increasing oscillations may appear. We neglect here the dynamics of the actuator, our goal being to show that the feed-back is able to provide a solution for the full model, using the trajectory planed with the simplified one, the linearizing outputs remaining close to their original values.

Unless otherwise stated, angles are expressed in radians, lengths in meters, times in seconds, thrusts in Newtons, masses in kg. Curves in red correspond to the planed trajectory $\hat{\xi}$, while curves in blue correspond to the integration of the full model. For more clarity z has been replaced by $-z$ to get positive values when drawing curves.

Computation times are real time, not cpu time, using Maple 19 with an Intel processor Core i5 2.5GHz. These are just indications that can vary from a session to an other one.

5.2 High angle of attack with the F16

We consider here with the models of the fighter F-16C linear horizontal trajectories at reduced speed in order to experiment high angle of attack, close to stalling. For both simulations, trajectory tracking is good, with variations for x less than 1m and for z less than 5m.

The F-16 has a thrust to weight ratio greater than 1 with afterburning. The highest thrust engine developped for it, the F110-GE-132, has a maximum thrust of $32,500$lbf (144.6kN), as the weight used in our computations is $20,500$lb. So, the only possibility for stalling is a maximum of $\tilde{Z}$, that occurs with the full model and the simplified one. The computed stall speed, angle of attack and thrust are 43.0408m/s (83.66kn), 0.7656rad ($43.87°$) and 47.8279KN, with the real model, 26.5681m/s, and 1.1957rad and 45.7808KN, with the simplified one. The angle of attack exceeds the limits of the model, but the evaluation with the full model is not so far from the real behaviour. Deep stalls with the F-16 have been reported at about 100kn with an angle of attack arround 50 to $60°$ (Dryden [6]). It corresponds to a loss of control that is difficult to escape and not just a loss of lift. The next fig. 11 provides the computed values of V and F depending on the angle of attack.

Figure 11: F-16: values of V and F depending on α, for the real and simplified models

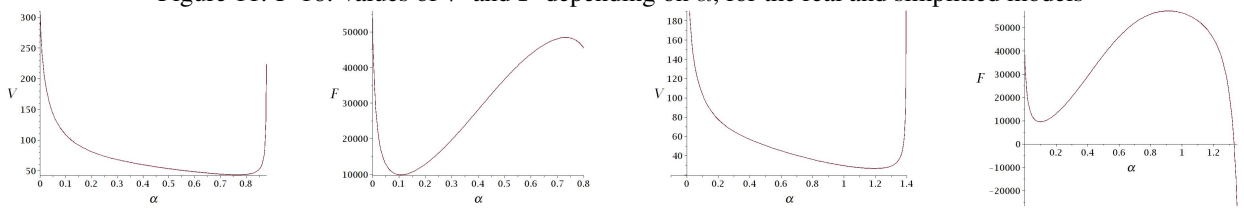

The following equations presents the value of the linearizing outputs and $\lambda_{i,j}$ used in the next simulation:

$$\begin{array}{ll} x & = 165t - 125.5\left(\int_0^t \operatorname{atan}\frac{x-60}{10}\mathrm{d}t - \int_0^t \operatorname{atan}\frac{x-120}{10}\mathrm{d}t\right)\mathrm{kn}; \\ y & = 0; \quad z = 0; \quad \mu = 0; \\ \lambda_{i,j} & = 0.5. \end{array} \tag{12}$$

In this simulation, the $\lambda_{i,j}$ are again small by necessity as the feed-back is close to its maximal possibilities. In the planed trajectory, the speed is reduced from 81.6650 at $t = 0$s (actually $V(0.2) = 81.66859$ is the initial maximum during simulation) to reach a minimum 44.48860 at $t = 90$ ($V(90.3 = 44.45203$m/s during simulation), then set back to the initial value ($V(180.) = 81.66516$ during simulation). The minimal speed is quite close to the computed stall speed for the full model: 43.0408m/s. The total computation time for the simulation is 294s. The total computation time for the simulation is 279s. See fig. 12

Figure 12: F-16 near stall speed: α, V, F, δ_m, δx and δz.

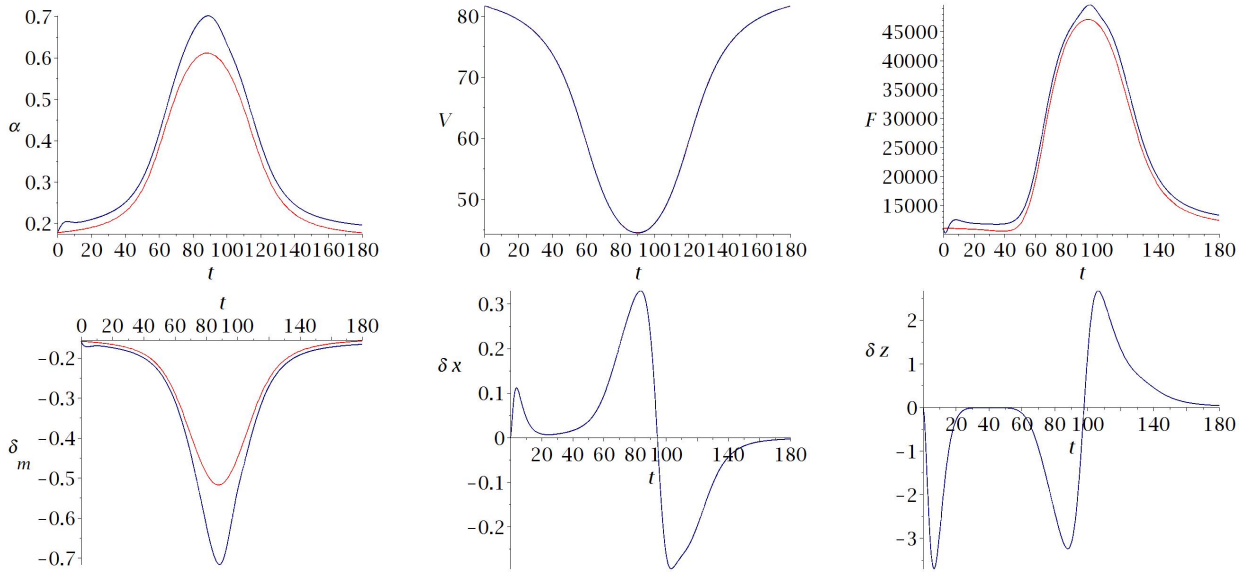

5.3 Gravity-free flight with the F16

We experiment here a 0-g flight with a parabolic trajectory. Among our models, only the F-16 and the GTM are avaible, for C_z does not vanish with the F4 and the T-O. See fig. 13. For this simulation, we used an expression of air density varying with altitude z, following Martin [23, A.16 p. 97]. The total computation time of the simulation is 371s.

$$\begin{array}{ll} x & = 750t\text{km/h}; \quad y = 0; \quad z = g\frac{t^2}{2} - 2000; \quad \mu = 0; \\ \eta & = 0; \\ \lambda_{i,j} & = 5.; \\ \rho & = 1.225(1 + 0.0065z/288.15)^{(9.80665/287.053\times 0.0065-1)} \end{array} \tag{13}$$

Figure 13: F-16 0-g flight: α, V, F, δ_m, δx and δz.

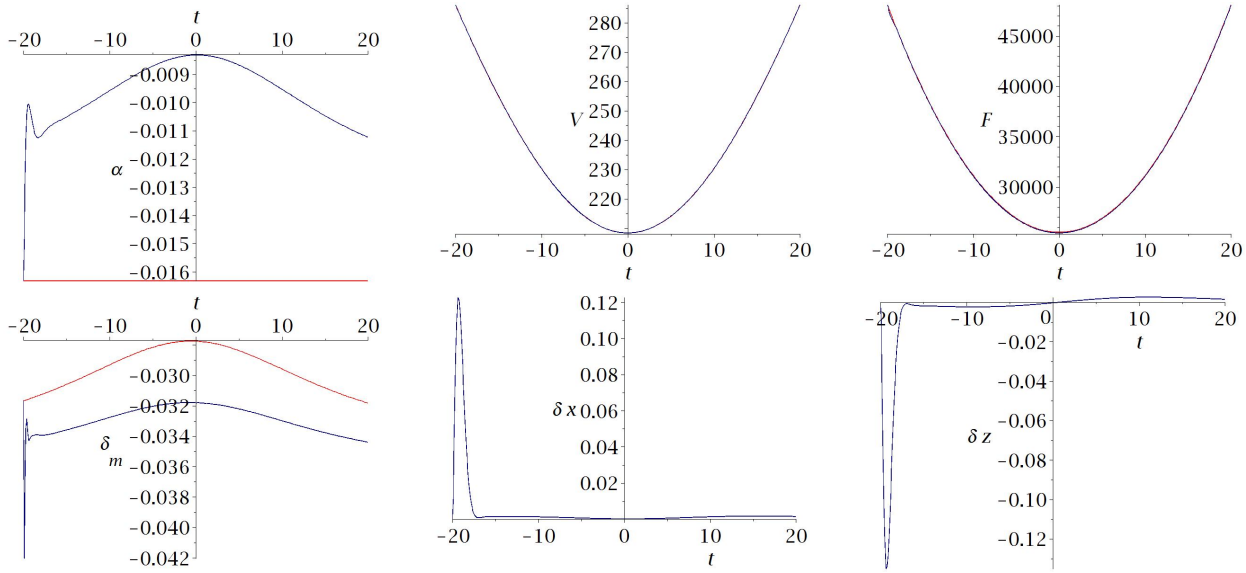

5.4 Twin Otter with one engine lost

We experiment here the Twin-Otter with one engine lost, with a progressive decrease of power. With the simplified model, μ and β both remain $zero$. It is no longer the case with the real domain, and we compare the case where the feed-back keeps μ or β close to 0.

The variation of β and μ are both 0 for the simplified model, so only the feed-back makes the difference, as the planed trajectory is the same when choosing β or μ in the linearizing outputs. We go from equal thrust to total extinction of starboard engine, setting the value of $\eta = (F_1 - F_2)/(F_1 + F_2)$ as in the equation below. So, the flat motion planning takes in account the extinction of one engine, which is not fully compensated by the feed-back as done in sec. 4. The distance of the engines to the plane of symmetry of the aircraft has been evaluated to $y_p = 9.2$ft.

$$\begin{array}{ll} x & = 140\text{kn}t; \quad y = 0; \quad z = 0; \quad \mu = 0; \\ \eta & = .5 + \frac{\text{atan}\frac{t-30.}{5.}}{\pi} \\ \lambda_{1,1} & = 1.,\ \lambda_{1,2} = 2.,\ \lambda_{1,3} = 3.,\ \lambda_{2,1} = 1.,\ \lambda_{2,2} = 1.,\ \lambda_{2,3} = 1.,\ \lambda_{2,4} = 2.,\ \lambda_{2,5} = 3., \\ \lambda_{3,1} & = 1.5,\ \lambda_{3,2} = 1.5,\ \lambda_{3,3} = 1.5,\ \lambda_{3,4} = 3.,\ \lambda_{4,5} = 4.,\ \lambda_{4,1} = 1.,\ \lambda_{4,2} = 2.,\ \lambda_{4,3} = 3. \end{array} \tag{14}$$

The Twin-Otter has generous control surfaces, making it highly manoeuvrable, but meaning a higher contribution of the δ_l, δ_m, δ_n to C_x, C_y and C_z. We need here to increase the λ_i, borrowing with some adaptations the values used by Martin [23].

The variations of μ and β remain little, in accordance with the reported hability of the T-O to fly with a single engine (Lecarme [17]). Setting $\mu = 0$ in the feedback, the values at the final time $t = 60$s of the simulation are $\beta = 0.05267$rad and $\mu = 0.105410^{-4}$rad with total computation time 71s for the simulation; setting $\beta = 0$, we get $\beta = -0.910^{-4}$rad and $\mu = -0.08974$rad with total computation time 93s for the simulation. See fig. 14 for μ and fig. 15 for β.

Figure 14: T-O single engine with β: α, V, F, δ_m, δx, δz, γ, q.

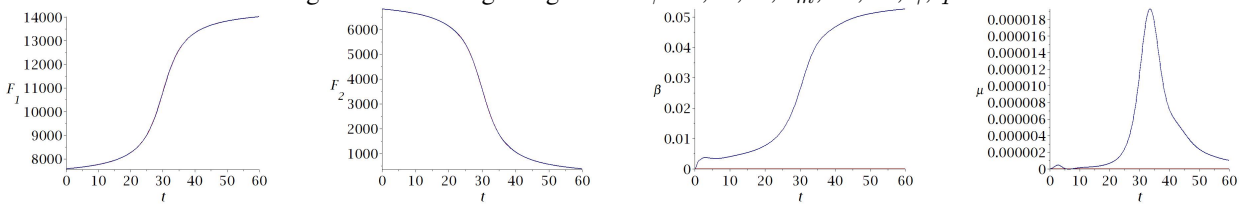

Figure 15: T-O single engine with β: α, V, F, δ_m, δx, δz, γ, q.

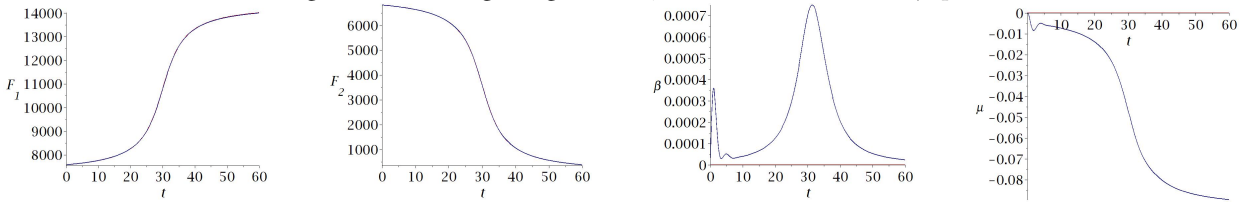

5.5 Rudder failure with the Twin Otter

We consider here differential thrust control of a T-O with rudder failure. We use flat outputs with β, and η is the control that replaces δ_n, set to $20°$. This constant value is taken in account in the simplified model. We use a descending near circular trajectory with speed close to 80kn.

$$\begin{array}{ll} x & = 1100\cos(\frac{80\text{kn}}{1100}t); \\ y = & 1200\sin(\frac{80\text{kn}}{1100}t); \\ z = & 5.5\text{ft}t + 0.025\text{ft}t^2 - 500; \\ \beta & = 0; \\ \lambda_{i,j} & = 5.5 \end{array} \tag{15}$$

The value of δ_n is set to $20°$ and η is used as a new control in order to simulate differential thrust control of the aircraft. The constant value of δ_n is used in the expression of C_x, C_y and C_z for the simplified model, only δ_l and δ_n being set to 0. The strong action of the controls during this circular trajectory implies a rather high value for all the $\lambda_{i,j}$. Precision is good, less to 2.2cm for δz and much less after oscillations during the first 10s of simultion. Nethertheless, small oscillations never stop for q and some other state functions. The T-O is the model for which designing a suitable feed-back is the most difficult. The maximal power for a single engine during the simulation is 537.4hp, bellow the maximal power 550shp (410 kW) of the Pratt & Whitney PT6A-20 engines of the T-O series 1, 100 and 200; the 300 series was fitted with PT6A-27 engines of 680hp (510kW), flat-rated to 620hp (460kW). The total computation time is 3500s. See fig. 16.

Figure 16: T-O rudder failure flight: α, β, μ, δx, δy, δz, $\delta\beta$, δ_m and F_1, F_2. One may notice the variations of μ and the control δ_m, due to the thrusts neglected in the simplified model.

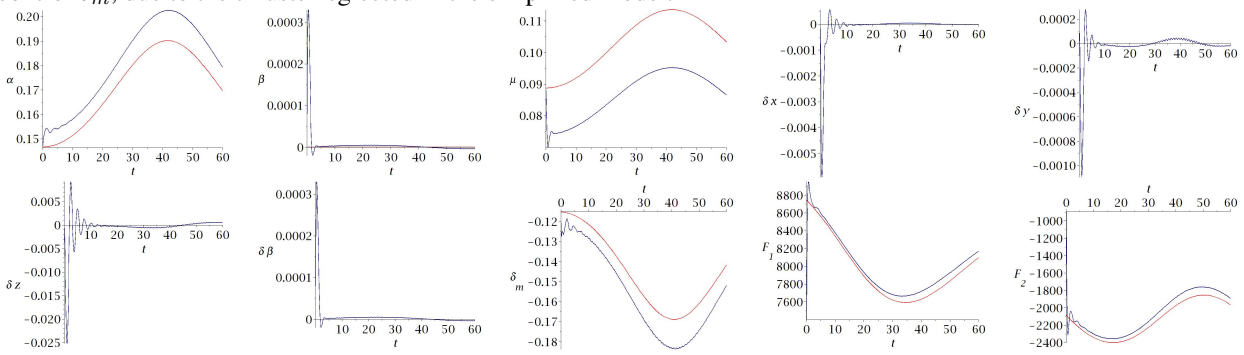

5.6 Landing and de-crab maneuver with the GTM

A decrab maneuver is considered here with the GTM. Two sets of curves are presented, the first for $-60 \leq t \leq -5$, the second to focus on the last 5sec. We use flat outputs with μ. The GTM is a $0,055$ scale model of a transport aircraft. We chose speeds that could match a real aircraft landing and multiply them by $0.055^{1/2}$. Lateral wind is set to $V_w := 30$km/h. The horizontal speed in the ground referential $\dot{x}$ is set to $\dot{x} = 135$kn at $t = -60$ and decreases to $V_0 := 120$kn on touchdown at $t = 0$. Near $t = 0$, the lateral acceleration, which was 0, is increased to reach at $t = 0$

$$\ddot{y} = G_y := \frac{\rho}{2m} S V_0^2 C_y(\beta_0),$$

with

$$\beta_0 := \text{atan} \frac{V_w}{(V_0^2 + V_w^2)},$$

so that the aircraft could land in the axis of the runway. The vertical speed is -20.5ft at $t = -60$ and decreases to -1.5ft at $t = 0$. The flat outputs and $\lambda_{i,j}$ are then as follows. We also used here expressions of C_x and C_z depending on z to take in account ground effect. For this, in (28), C_D is replaced with $\Phi(z)C_D$ and we substitute to α in C_L the value $-\theta_{16}/\theta_{17} + (\theta_{16}/\theta_{17} + \alpha)/\Phi(z)$, where $\Phi(z) = (16.z/a)^2/(1 + (16.z/a)^2)$, using McCormick formula. See Gudmundsson [11, (9-66) p. 351]. These empirical formulas should roughly match ground effect, but have no claim for physical pertinence. They are just meant to demonstrate the hability of our implementation to handle such expressions when needed.

The aircraft is assumed to land when z is equal to the length of the landing gear, evaluated to 17cm. Without precise data for the GTM parameters in landing conditions, drag and lift have been empirically increased. The value of coefficient θ_1, the constant term of C_D, has been changed from $\theta_1 = 0.019$ to $\theta_1 = 0.019 + 0.02$ and θ_{16}, the constant term of C_L has been changed from $\theta_{16} = 0.016$ $\theta_{16} = 0.016 + 2.02$.

$$\begin{array}{lll} x & = 0.055^{1/2} int_0^t \left(135\text{kn} - 15\text{kn}\left(.5 + \frac{\text{atan}\frac{\tau+25}{20.}}{\pi}\right)\right) \text{d}\tau; \\ y = & G_y \frac{\int_{-60}^t \int_{-60}^\tau \left(.5 + \frac{\text{atan}\frac{\theta+1.5}{.5}}{\pi}\right) \text{d}\tau \text{d}t}{0.5 + \text{atan}(25/20)}; \\ z = & 0.055^{1/2} \left(1.5\text{ft}t + \int_0^t .5 - \text{atan}\frac{x+25.}{20.}\pi 19.\right) \text{ft}; \\ \beta & = 0; \\ \lambda_{i,j} & = 5.5 \end{array} \tag{16}$$

Using quite great values for the λ allows a greater precision in following the flat outputs, but implies oscillations during the first 5s of simulation. It is mostly required during the decrab which is too fast to allow a weaker control.

Figure 17: GTM decrab maneuver from -60sec to -5sec: α, β, μ, δx, δy, δz, δ_m and F.

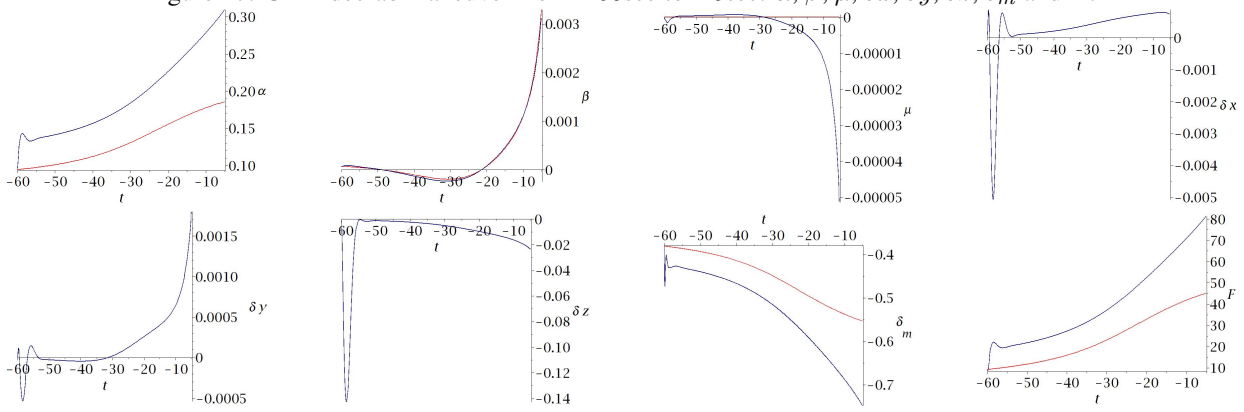

Touch down is done a little before $t = 0$, at $t = -0.18$, when z becomes equal to the length of landing gears. The value of μ is -0.510^{-2}. The horizontal speed has a deviation of $-2.6762°$ with respect to the runway axis, and the aircraft body a deviation $-0.932967°$. Speeds are given in m/s, divided by $0.55^{-1/2}$ to match real aircraft data. The vertical speed is thus 1.39764m/s and the horizontal speed 63.2158m/s.

The total computation time for these simulations is 752s. See fig. 17 and 18.

Figure 18: GTM decrab maneuver from -5sec to 0sec: α, β, μ, δx, δy, δz, δ_m and F.

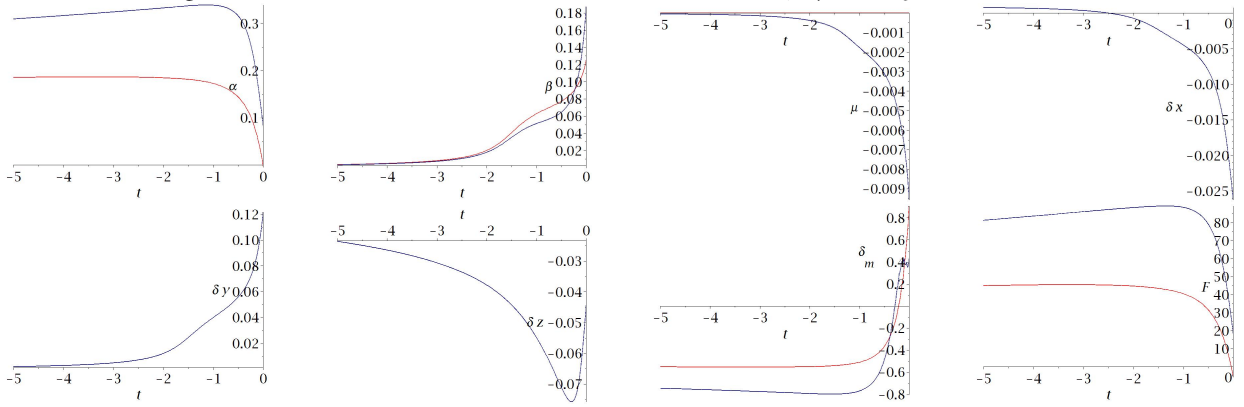

5.7 Forward slip with the GTM

Special maple packages have been designed to model gliding. Basically, the structure remained unchanged, except that all variable related to the thrust are no longer needed, and that we only have 3 flat outputs. The only change in the GTM model was setting the gravity center position x_{cg} to 0., to make things a little easier. Anyway, we could not succeed to design a feed-back allowing to follow a straight-line trajectory. This is due to the contribution of the controls δ_l, δ_m and δ_n to drag and lift terms. To solve this issue, instead of setting them to 0. in the simplified model, we just used values compatible with the mean speed and flight path angle of the chosen trajectory.

The following table shows constant values for straight line trajectories, depending on α and β, for both the real and the simplified model with $(p, q, r, \delta_\ell, \delta_m, \delta_n) = (0, 0, 0, 0, 0, 0)$.

Model	α	β	γ	μ	V	δ_l	δ_m	δ_n	V_x	V_y
Simple	0.15	0.	-0.1187	0.	29.8996	0.	0.	0.	29.6890	3.5425
Real	0.15	0.	-0.1190	0.	30.3053	0.	-0.0490	0.	30.0908	3.5992
Simple	0.15	0.2	-0.1650	0.2409	29.3672	0.	0.	0.	28.9679	4.8262
Real	0.15	0.2	-0.1470	0.1345	30.1114	-0.1880	-0.0490	0.3305	29.7864	4.4120
Simple	0.15	0.35	-0.2508	0.3899	28.4019	0.	0.	0.	27.5129	7.0503
Real	0.15	0.35	-0.2027	.2250	29.7171	-0.3316	-0.0490	0.5690	29.1085	5.9832

We see that the controls δ_l, δ_m and δ_n increases with β and cannot be neglected for values of β great enough to allow a flat parametrization. For our simulation, we have chosen $\alpha = 0.15$ and $\beta = 0.35$ as reference value and set the value of the controls in C_x, C_y and C_z according to the abobe table. To fix ideas, the speed values for a 0.055 scale model such as the GTM must be divided by $0.055^{0.5}$ to get full scale values. This gives 456.1709km/h for the total speed and 25.51m/s for the vertical speed (83.70ft/s).

Here are the flat output trajectories and feedback parameters.

$$\begin{array}{ll} x & = 29.10852587t + 50\sin(t/60.); \\ y & = 60\cos(t/100. + 2.); \\ z & = -1000 + 5.983293200t + 70\sin(t/70.)); \\ \lambda_{i,j} & = 0.5 \end{array} \tag{17}$$

The total computation time is 157s for this simulation. See figure 19 bellow.

Figure 19: GTM forward slip maneuver from 0sec to 60sec: α, β, μ, δx, δy, δz, δ_l, δ_m and δ_n.

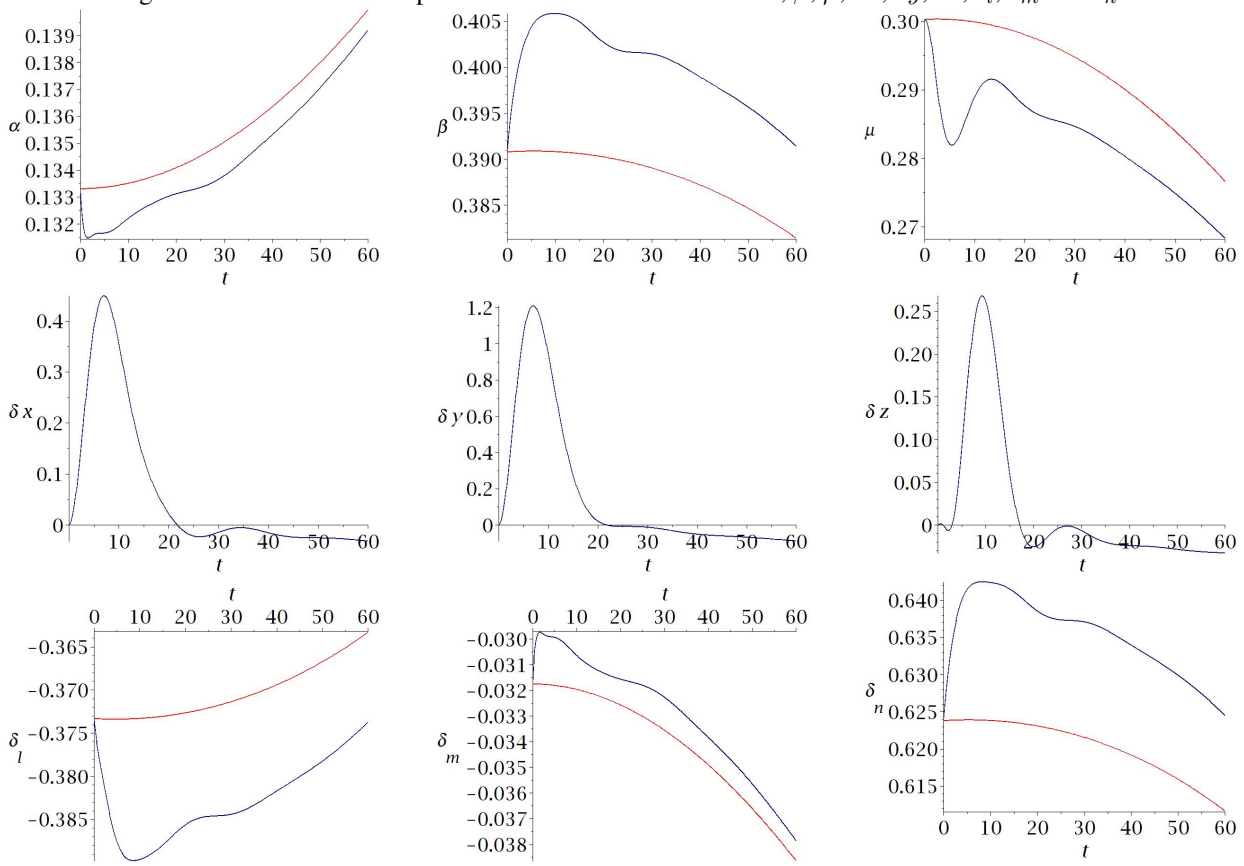

This simulation has obviously no claim to be realistic, but is just meant to illustrate the computational possibilities of our methods, that can be improved in many ways to take better account of actual situations.

Conclusion

We have seen that flat control could be used with some reliability, even in some situations where the validity of the required simplifications in the equations can be questionned, and in various failure conditions.

This research shows how a non-flat system can be controlled by a suitable feedback along a trajectory designed for a flat approximation. This raises numerous theoretical questions concerning the convergence of such a procedure in a general setting and the meaning and interpretation of the limit trajectory, that have been sketched in [28] and will be addressed in future works.

References

[1] ASSELIN (Mario), *An Introduction to Aircraft Performance*, American Institute of Aeronautics and Astronautics, Inc., 1997.

[2] BURCHAM JR. (Frank W.), BURKEN (John J.), MAINE (Trindel A.) and BULL (John), "Emergency Flight Control Using Only Engine Thrust and Lateral Center-of-Gravity Offset: A First Look", *Joint propulsion conference* 1997. NASA Technical Memorandum 4798

[3] BURCHAM JR. (Frank W.), MAINE (Trindel A.) and BURKEN (John J.), *Using Engine Thrust for Emergency Flight Control: MD-lI and B-747 Results*, NASA Dryden Flight Research Center, Technical Memorandum 206552, 1998.

[4] BURCHAM JR. (Frank W.), FULLERTON, (Charles Gordon) and MAINE (Trindel A.), *Manual Manipulation of Engine Throttles for Emergency Flight Control*, NASA Dryden Flight Research Center, Technical Memorandum 212045, 2004.

[5] "The flight crew of an A300 hit by a missile shortly after take-off manage to turn their aircraft around and put it down safely", *Flight Savety Australia*, Civil Aviation Safety Authority, 2004.

[6] DRYDEN (Joe Bill), "Recovering From Deep Stalls And Departures", *Code One*, July 1986.

[7] FLIESS (Michel), LÉVINE (Jean), MARTIN (Philippe) and ROUCHON (Pierre), "Défaut d'un système non linéaire et commande haute fréquence", C. R. Acad. Sci. Paris, Automatique t. 316, Série I, p. 513-518, 1993.

[8] FLIESS (Michel), LÉVINE (Jean), MARTIN (Philippe) and ROUCHON (Pierre), "Flatness and defect of nonlinear systems: introductory theory and examples", International Journal of Control, Vol. 61, No. 6, p.1327–1361, 1995.

[9] FLIESS (Michel), LÉVINE (Jean), MARTIN (Philippe) and ROUCHON (Pierre), "A Lie-Bäcklund approach to equivalence and flatness of nonlinear systems", *IEEE Trans. Automat. Control*, Vol. 44, n° 5, 922–937, 1999.

[10] GRAUER (Jared A.) and MORELLI (Eugene A.), "A generic nonlinear aerodynamic model for aircraft", *AIAA Atmospheric Flight Mechanics Conference*, 2014.

[11] GUDMUNDSSON (Snorri), *General aviation aircraft design: applied methods and procedures*, Butterworth-Heinemann (Elsevier), Oxford, 2014.

[12] HUESCHEN (R.M.), *Development of the Transport Class Model (TCM) Aircraft Simulation From a Sub-Scale Generic Transport Model (GTM) Simulation*, NASA/TM–2011-217169, 2011.

[13] HANNAN (Muhammad Abdul), WANG (Shaoping) and WANG (Xingjian), "Fault tolerant control based on differential engine thrust and ailerons of a damaged aircraft with vertical tail loss", *14th International Bhurban Conference on Applied Sciences and Technology (IBCAST)*, Islamabad, 305–311, 2017.

[14] JAKUBCZYK (Bronisław) and RESPONDEK (Witold), "On linearization of control systems", *Bull. Acad. Pol. Sci. Ser. Sci. Math.*, vol. 28, (9-10), 517–522, 1980.

[15] KAMINSKI (Yirmeyahu J.), LÉVINE (Jean) and OLLIVIER (François), "Intrinsic and apparent singularities in flat differential systems and application to global motion planning", *Systems & Control Letters*, vol. 113, 117–124, 2018.

[16] KAMINSKI (Yirmeyahu J.), LÉVINE (Jean) and OLLIVIER (François), "On Singularities of Flat Affine Systems With n States and $n-1$ Controls", *International Journal of Robust and Nonlinear Control*, vol. 30, n^o 9, Wiley, 3547–3565, 2020.

[17] LECARME (Jacques), "Lignes de vol, le De Havilland DHC-6 Twin Otter", *Aviation Magazine* n^o 449, 1966.

[18] LÉVINE (Jean), *Analysis and Control of Nonlinear Systems: A Flatness-based Approach*, Springer, 2009.

[19] LÉVINE (Jean), "On necessary and sufficient conditions for differential flatness", *Applicable Algebra in Engineering, Computation and Communication*, 27–90, 2011.

[20] LOCKWOOD (George H.), *Final report of the board of inquiry into Air Canada Boeing 767 C-GAUN Accident — Gimli, Manitoba, July 23, 1983*, Canadian Government Publishing Center, 1985.

[21] LU (Long K.) and TURKOGLU (Kamran), "Adaptive Differential Thrust Methodology for Lateral/Directional Stability of an Aircraft with a Completely Damaged Vertical Stabilizer", *International Journal of Aerospace Engineering*, volume 2018.

[22] MCLEAN (Donald), *Automated flight control systems*, Prentice Hall, New York, 1990.

[23] MARTIN (Philippe), *Contribution à l'étude des systèmes différentiellement plats*, Ph.D. Thesis, École des Mines de Paris, 1992.

[24] MARTIN (Philippe), "Aircraft Control Using Flatness", *IMACS/IEEE-SMC Multiconference CESA'96 – Symposium on Control, Optimization and Supervision*, CESA, 194–199, 1996.

[25] *Aircraft Accident Report NTSB/AAR-73-02: American Airlines, Inc. McDonnell Douglas DC-10-10, N103AA. Near Windsor, Ontario, Canada. 12 June 1972*, National Transportation Safety Board, February 28, 1973.

[26] *Loss of Thrust in Both Engines After Encountering a Flock of Birds and Subsequent Ditching on the Hudson River US Airways Flight 1549 Airbus A320-214, N106US Weehawken, New Jersey January 15, 2009*, Accident Report NTSB/AAR-10/03, National Transportation Safety Board, 2010.

[27] *NATOPS flight manual, navy model, F-4F aircraft*, Change 2, NATOPS, 1978.

[28] OLLIVIER (François), "Extending Flat Motion Planning to Non-flat Systems. Experiments on Aircraft Models Using Maple", to appear in *Proceedings of the 2022 International Symposium on Symbolic and Algebraic Computation (ISSAC '22)*, July 4–7, 2022, Villeneuve-d'Ascq, France.

[29] KRASIL'SHCHIK (Iosif Semenovitch), LYCHAGIN (Valentin V.) and VINOGRADOV (Alexandre Mikhailovich), *Geometry of Jet Spaces and Nonlinear Partial Differential Equations*, Gordon and Breach, New York, 1986.

[30] ZHARINOV (Victor V.), *Geometrical aspects of partial differential equations*, Series on Soviet and East European Mathematics, vol. 9, World Scientific, Singapore, 1992.

A Nomenclature

Roman

a: wing span

C_x, C_y, C_z: aerodynamic force coefficients, wind frame

C_D, C_L: lift and drag coefficient in aircraft frame

C_l, C_m, C_n: aerodynamic moment coefficients

c: mean aerodynamic chord

F: thrust

L, M, N: aerodynamic moments

m: mass

p, q, r: roll, pitch and yaw rates

S: wing area

V: airspeed

X, Y, Z: aerodynamic forces

y_p: distance of the engines to the plane of symmetry

Greek

α angle of attack

β sideslip angle

γ: flight path angle

η: differential thrust ratio

ϑ: pitch angle

θ: parameters

μ: bank angle

ϕ: roll angle

χ: aerodynamic azimuth or heading angle

ψ: yaw angle

δ_l, δ_m, δ_n: aileron, elevator, rudder deflexion

θ: model parameters

B Aircraft Model

The model presented here relies on Martin [23, 24]. On may also refer to Asselin [1], Gudmundsson [11] or McLean [22] for more details.

B.1 Earth frame, wind frame and body frame

We use an earth frame with origin at ground level, with z-axis pointing downward, as in the figure 20 (left). The coordinates of the gravity center of the aircraft are given in this referential.

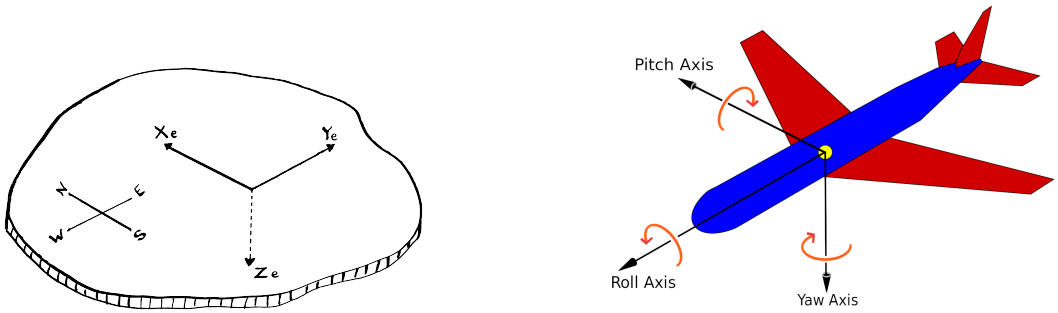

Figure 20: Earth frame and body frame.

The body frame or aircraft referential is defined as in figure 20 (right), where x_b corresponds to the roll axis, y_b to the pitch axes and z_b to the yaw axes, oriented downward. The angular velocity vector (p, q, r) is given in this referential, or to be more precise, at each time, in the Galilean referential that is tangent to this referential.

We go from earth referential to body referential using first a rotation with respect to z axis by the yaw angle ψ, then a rotation with respect to y axis by the pitch angle ϑ, and last a rotation with respect to x axis by the roll angle ϕ, which gives a rotation matrix:

$$R_{eb} = \begin{bmatrix} \cos(\psi(t))\cos(\vartheta(t)) & \sin(\phi(t))\sin(\vartheta(t))\cos(\psi(t)) - \sin(\psi(t))\cos(\phi(t)) & \sin(\phi(t))\sin(\psi(t)) + \sin(\vartheta(t))\cos(\phi(t))\cos(\psi(t)) \\ \sin(\psi(t))\cos(\vartheta(t)) & \sin(\phi(t))\sin(\psi(t))\sin(\vartheta(t)) + \cos(\phi(t))\cos(\psi(t)) & -\sin(\phi(t))\cos(\psi(t)) + \sin(\psi(t))\sin(\vartheta(t))\cos(\phi(t)) \\ -\sin(\vartheta(t)) & \sin(\phi(t))\cos(\vartheta(t)) & \cos(\phi(t))\cos(\vartheta(t)) \end{bmatrix}. \tag{18}$$

The wind frame, with origin the center of gravity of the aircraft has an axis x_w, in the direction of the velocity of the aircraft, the axis z_w being in the plane of symmetry of the aircraft. The Euler angles that define the orientation of the wind frame in the earth frame are denoted $\chi(t), \gamma(t), \mu(t)$, and are respectively the *aerodynamic azimuth* or *heading angle*, the *flight path angle* and the *aerodynamic bank angle*, positive if the port side of the aircraft is higher than the starboard side. See figure 21 (left). We go from earth referential to wind referential using first a rotation with respect to

z axis by the *heading angle* χ, then a rotation with respect to y axis by the *flight path angle* γ, and last a rotation with respect to x axis by the *bank angle* μ, which gives a rotation matrix:

$$R_{ew} = \begin{bmatrix} \cos(\chi(t))\cos(\gamma(t)) & \sin(\mu(t))\sin(\gamma(t))\cos(\chi(t)) - \sin(\chi(t))\cos(\mu(t)) & \sin(\mu(t))\sin(\chi(t)) + \sin(\gamma(t))\cos(\mu(t))\cos(\chi(t)) \\ \sin(\chi(t))\cos(\gamma(t)) & \sin(\mu(t))\sin(\chi(t))\sin(\gamma(t)) + \cos(\mu(t))\cos(\chi(t)) & -\sin(\mu(t))\cos(\chi(t)) + \sin(\chi(t))\sin(\gamma(t))\cos(\mu(t)) \\ -\sin(\gamma(t)) & \sin(\mu(t))\cos(\gamma(t)) & \cos(\mu(t))\cos(\gamma(t)) \end{bmatrix}. \tag{19}$$

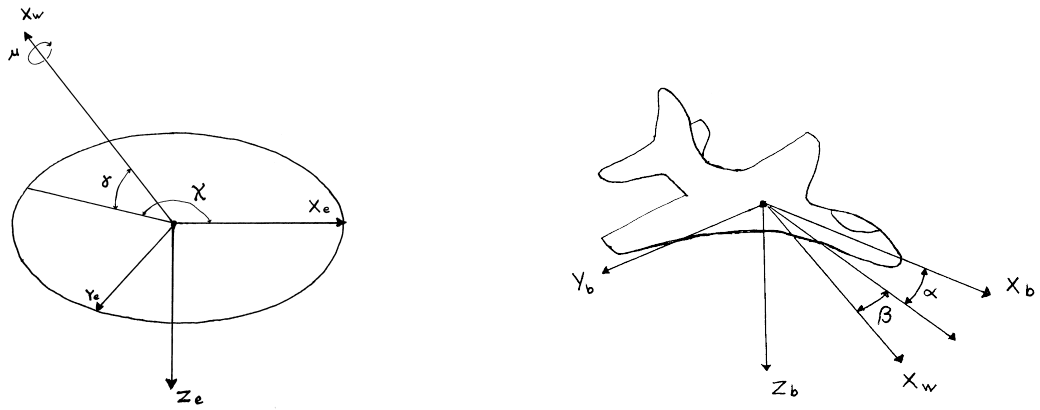

Figure 21: Wind frame and body frame.

The orientation of the wind frame with respect to the body frame is defined by two angles: the *angle of attack* $\alpha(t)$ and the *sideslip angle* $\beta(t)$, which is positive when the wind is on the starboard side of the aircraft, as in figure 21 (right). We go from the wind referential to the body referential using first a rotation with respect to z axis by the side slip angle β and then a rotation with respect to y axis by the angle of attack α, which gives a rotation matrix:

$$R_{wb} = \begin{bmatrix} \cos(\alpha(t))\cos(\beta(t)) & \sin(\beta(t)) & \sin(\alpha(t))\cos(\beta(t)) \\ -\sin(\beta(t))\cos(\alpha(t)) & \cos(\beta(t)) & -\sin(\alpha(t))\sin(\beta(t)) \\ -\sin(\alpha(t)) & 0 & \cos(\alpha(t)) \end{bmatrix}. \tag{20}$$

B.2 Dynamics

In the sequel, we shall write $p(t), q(t), r(t)$ the coordinates of the rotation vector of the body frame with respect to the the earth frame expressed in the Galilean referential that coincide at time t with the body frame, and $L(t)$, $M(t)$, $N(t)$ the corresponding torques. In the same way $X(t)$, $Y(t)$ and $Z(t)$ denote the forces applied on the aircraft, expressed in the Galilean referential that coincide at time t with the the wind referential.

B.2.1 Aircraft geometry

The mass of the aircraft is denoted by m, S is the surface of the wings. In the body frame, we assume that the aircraft is symmetrical with respect to the xz-plane, so that the tensor of inertia has the following form:

$$J := \begin{bmatrix} I_{xx} & 0 & -I_{xz} \\ 0 & I_{yy} & 0 \\ -I_{xz} & 0 & I_{zz} \end{bmatrix}. \tag{21}$$

In the standard equations (27), we also need a, that stands for the *wing span* and b for the *mean aerodynamic chord*.

B.2.2 Forces and torques

The forces and torques exerted on the aircraft can be easily enumerated:

1. Propulsion force F and torque T_p, which is the sum of the propulsion force and torque of each reactor: $F = F_1 + F_2$ and T_p proportional to $y_p(F_1 - F_2)$, where y_p is the distance of the engines to the plane of symmetry;

2. Aerodynamic force and torque

$$F_a = \rho/2SV^2C_f, \text{ with } C_f = (C_x, C_y, C_z)^{\mathrm{t}} \tag{22a}$$

$$T_a = \rho/2SV^2C_t, \text{ with } C_t = (C_\ell, C_m, C_n)^{\mathrm{t}} \tag{22b}$$

where ρ is the volumetric mass of air;

3. Weight: gm, which gives no torque.

The force (X, Y, Z) in the wind frame and the torque (L, M, N) are then expressed by the next formulas:

$$X = F(t)\cos(\alpha+\epsilon)\cos(\beta(t)) - \frac{\rho}{2}SV(t)^2C_x - gm\sin(\gamma(t)); \tag{23a}$$

$$Y = F(t)\cos(\alpha+\epsilon)\sin(\beta(t)) + \frac{\rho}{2}SV(t)^2C_y + gm\cos(\gamma(t))\sin(\mu(t)); \tag{23b}$$

$$Z = -F\sin(\alpha+\epsilon) - \frac{\rho}{2}SV(t)^2C_z + gm\cos(\gamma(t))\cos(\mu(t)); \tag{23c}$$

$$L = -y_p\sin(\epsilon)(F_1(t) - F_2(t)) + \frac{\rho}{2}SV(t)^2aC_l; \tag{23d}$$

$$M = \frac{\rho}{2}SV(t)^2bC_m; \tag{23e}$$

$$N = y_p\cos(\epsilon)(F_1(t) - F_2(t)) + \frac{\rho}{2}SV(t)^2aC_n. \tag{23f}$$

The angle ϵ is related to the lack of parallelism of the reactors with respect to the $xy-$plane in the body frame and is small. In the last expressions, we leave the terms depending on ϕ and ϑ for simplicity, but in our computations they are replaced by their expressions depending on γ, μ, α and β, using $R_{eb} = R_{wb}R_{ew}$.

The aerodynamic coefficients $C_x, C_y, C_z, C_l, C_m, C_n$ depend on α and β and also on the angular speeds p, q, r and the controls are virtual angles δ_l, δ_m and δ_n, that respectively express the positions of the ailerons, elevator and rudder.

B.2.3 Equations

Following Martin [23, 24], the dynamics of the system is modeled by the following set of explicit differential equations (24a–24i,25):

$$\frac{d}{dt}x(t) = V(t)\cos(\chi(t))\cos(\gamma(t)); \tag{24a}$$

$$\frac{d}{dt}y(t) = V(t)\sin(\chi(t))\cos(\gamma(t)); \tag{24b}$$

$$\frac{d}{dt}z(t) = -V(t)\sin(\gamma(t)); \tag{24c}$$

$$\frac{d}{dt}V(t) = \frac{X}{m}; \tag{24d}$$

$$\frac{d}{dt}\gamma(t) = -\frac{Y\sin(\mu(t)) + Z\cos(\mu(t))}{mV(t)}; \tag{24e}$$

$$\frac{d}{dt}\chi(t) = \frac{Y\cos(\mu(t)) - Z\sin(\mu(t))}{\cos(\gamma(t))mV(t)}; \tag{24f}$$

$$\begin{aligned}\frac{d}{dt}\alpha(t) = \ & \tfrac{1}{\cos(\beta(t))}(-p\cos(\alpha(t))sin(\beta(t)) \\ & +q\cos(\beta(t)) - r\sin(\alpha(t))\sin(\beta(t)) + \tfrac{Z}{mV(t)});\end{aligned} \tag{24g}$$

$$\frac{d}{dt}\beta(t) = +p\sin(\alpha(t)) - r\cos(\alpha(t)) + \frac{Y}{mV(t)}; \tag{24h}$$

$$\begin{aligned}\frac{d}{dt}\mu(t) = \ & \tfrac{1}{\cos(\beta(t))}(p\cos(\alpha(t)) + r\sin(\alpha(t)) \\ & +\tfrac{1}{mV(t)}(Y\cos(\mu(t))\tan(\gamma(t))\cos(\beta(t)) - Z(\sin(\mu(t))\tan(\gamma(t))\cos(\beta(t)) + sin(\beta(t)))));\end{aligned} \tag{24i}$$

$$\begin{pmatrix} \frac{d}{dt}p(t) \\ \frac{d}{dt}q(t) \\ \frac{d}{dt}r(t) \end{pmatrix} = J^{-1} \begin{pmatrix} (I_{yy} - Izz)qr + I_{xz}pq + L \\ (I_{zz} - I_{xx})pr + I_{xz}(r^2 - p^2) + M \\ (I_{xx} - I_{yy})pq - I_{xz}rq + N \end{pmatrix}. \tag{25}$$

We recall that in the last expressions, the terms depending on gravity do not appear as in Martin [23], but have been incorporated to the expressions X, Y and Z, as in [24].

We notice with Martin that this set of equations imply $\cos(\beta)\cos(\gamma)V \neq 0$. The non vanishing of V and $\cos(\beta)$ seems granted in most situations; the vanishing of V may occur with aircrafts equipped with vectorial thrust, which means a larger set of controls, that we won't consider here. The vanishing of $\cos(\gamma)$ can occur with loopings etc. and would require the choice of a second chart with other sets of Euler angles.

B.3 The GNA model

In the last equations, ρ can depend on z, as the air density vary with altitude. The expression of C_x and C_z could also depend on z to take in account ground effect. These expressions that depend on α, β, p, q, r, δ_l, δ_m and δ_n, should also depend on the Mach number, but most available formulas are given for a limited speed range and the dependency on V is limited to the V^2 term in factor. In the literature, the available expressions are often partial or limited to linear approximations. McLean [22] provides such data for various types of aircrafts; for different speed and flight conditions, including landing conditions with gears and flaps extended.

We have chosen here to use the Generic Nonlinear Aerodynamic (GNA) subsonic models, given by Grauer and Morelli [10] that cover a wider range of values, given in the following table.

$-4^\circ \leq \alpha \leq 30^\circ$,	$-20^\circ \leq \beta \leq 20^\circ$,	
$-100^\circ/\text{s} \leq p \leq 100^\circ/\text{s}$,	$-50^\circ/\text{s} \leq q \leq 50^\circ/\text{s}$,	$-50^\circ/\text{s} \leq r \leq 50^\circ/\text{s}$,
$-10^\circ \leq \delta_l \leq 10^\circ$,	$-20^\circ \leq \delta_m \leq 10^\circ$,	$-30^\circ \leq \delta_n \leq 30^\circ$

(26)

Among the 8 aircrafts in their database, we have made simulations with 4: fighters F-4 and F-16C, STOL utility aircraft DHC-6 Twin Otter and the sub-scale model of a transport aircraft GTM (see [12]).

The GNA model depends on 45 coefficients:

$$\begin{array}{rcl} C_D &=& \theta_1 + \theta_2\alpha + \theta_3\alpha\tilde{q} + \theta_4\alpha\delta_m + \theta_5\alpha^2 + \theta_6\alpha^2\tilde{q} + \theta_7\delta_m + \theta_8\alpha^3 + \theta_9\alpha^3\tilde{q} + \theta_{10}\alpha^4, \\ C_y &=& \theta_{11}\beta + \theta_{12}\tilde{p} + \theta_{13}\tilde{r} + \theta_{14}\delta_l + \theta_{15}\delta_n, \\ C_L &=& \theta_{16} + \theta_{17}\alpha + \theta_{18}\tilde{q} + \theta_{19}\delta_n + \theta_{20}\alpha\tilde{q} + \theta_{21}\alpha^2 + \theta_{22}\alpha^3 + \theta_{23}\alpha^4, \\ C_l &=& \theta_{24}\beta + \theta_{25}\tilde{p} + \theta_{26}\tilde{r} + \theta_{27}\delta_l + \theta_{28}\delta_n \\ C_m &=& \theta_{29} + \theta_{30}\alpha + \theta_{31}\tilde{q} + \theta_{32}\delta_e + \theta_{33}\alpha\tilde{q} + \theta_{34}\alpha^2\tilde{q} + \theta_{35}\alpha^2\delta_e + \theta_{36}\alpha^3\tilde{q} + \theta_{37}\alpha^3\delta_e + \theta_{38}\alpha^4, \\ C_n &=& \theta_{39}\beta + \theta_{40}\tilde{p} + \theta_{41}\tilde{r} + \theta_{42}\delta_l + \theta_{43}\delta_n + \theta_{44}\beta^2 + \theta_{45}\beta^3, \end{array} \tag{27}$$

where $\tilde{p} = ap$, $\tilde{r} = ar$, $\tilde{q} = bq$ (see B.2.1 for the meaning of a and b), C_D and C_L correspond to the lift and drag coefficients in the aircraft frame. The coefficients C_x and C_z in the wind frame are then obtained by the formulas:

$$\begin{array}{rcl} C_x &=& \cos(\alpha)C_D + \sin(\alpha)C_L, \\ C_z &=& \cos(\alpha)C_L - \sin(\alpha)C_D. \end{array} \tag{28}$$

B.4 Parametrization

Using the simplified model, $\dot{\Xi}_i$ only depends on $\Xi_1, \ldots, \Xi_{i+1}$, for $i < 4$, so that the model is chained, as already said in subsec. 1.3.

B.4.1 Computing Ξ_2

We have:

$$V = \sqrt{\dot{x}^2 + \dot{y}^2 + \dot{z}^2}; \tag{29a}$$

$$\chi = \text{atan2}(\dot{y}, \dot{x}); \tag{29b}$$

$$\gamma = \text{asin}\left(\frac{\dot{z}}{\sqrt{\dot{x}^2 + \dot{y}^2}}\right), \tag{29c}$$

expressions that are defined and $\mathcal{C}^\infty$ whenever $\dot{x}^2 + \dot{y}^2 \neq 0$. A change of charts is required in principle when $\chi = -\pi + 2k\pi$, $k \in \mathbb{Z}$. In practice, a carefull implementation is able to add 2π or -2π to keep the expression continuous, when following a trajectory.

B.4.2 Computing Ξ_3

It is now easilly seen from eq. (24d–24f) that $\dot{\Xi}_2$ is linear in X, $\sin\mu\, Y + \cos\mu\, Z$ and $\cos\mu\, Y - \sin\mu\, Z$, so that these quantities may be computed, knowing Ξ_1, Ξ_2, $\dot{\Xi}_2$. Starting from this point, the singularities of some choices of flat outputs are discussed in sec. 2.

B.4.3 Computing Ξ_4

We may then continue the same process. By equations (24g,24h,24i), which are linear in p, q and r, we see that p, q and r can be computed knowing (x, y, z) and their derivatives up to order 3, provided that the state variables in $\bigcup_{i=1}^{3} \Xi_i$ can be computed.

B.4.4 Computing Ξ_5

On the other hand, the coefficients C_l, C_m, C_n respectively strongly depend on $\delta_l, \delta_m, \delta_n$, as the torques L, M and N are mostly determined by the position of the ailerons, elevators and rudder. So, we have

$$\begin{vmatrix} \frac{\partial \dot{p}}{\partial \delta_l} & \frac{\partial \dot{p}}{\partial \delta_m} & \frac{\partial \dot{p}}{\partial \delta_n} \\ \frac{\partial \dot{q}}{\partial \delta_l} & \frac{\partial \dot{q}}{\partial \delta_m} & \frac{\partial \dot{q}}{\partial \delta_n} \\ \frac{\partial \dot{r}}{\partial \delta_l} & \frac{\partial \dot{r}}{\partial \delta_m} & \frac{\partial \dot{r}}{\partial \delta_n} \end{vmatrix} \neq 0.$$

The same is true if δ_n is replaced by η, which appears linearly in N (see (23f)). Then, we have in the same way:

$$\begin{vmatrix} \frac{\partial \dot{p}}{\partial \delta_l} & \frac{\partial \dot{p}}{\partial \delta_m} \\ \frac{\partial \dot{q}}{\partial \delta_l} & \frac{\partial \dot{q}}{\partial \delta_m} \end{vmatrix} \neq 0.$$

B.4.5 Conclusion

In conclusion, flat outputs x, y, z and $\zeta(\alpha, \beta, \mu, F)$ are regular if

i) $\dot{x}^2 + \dot{y}^2 \neq 0$, a problem that could be solved by a change of charts, provided that$\dot{x}^2 + \dot{y}^2 + \dot{z}^2 \neq 0$, and

ii) if α, β, μ and F can be localy expressed as functions of X, $\sin\mu\, Y + \cos\mu\, Z$, $\cos\mu\, Y - \sin\mu\, Z$ and ζ.